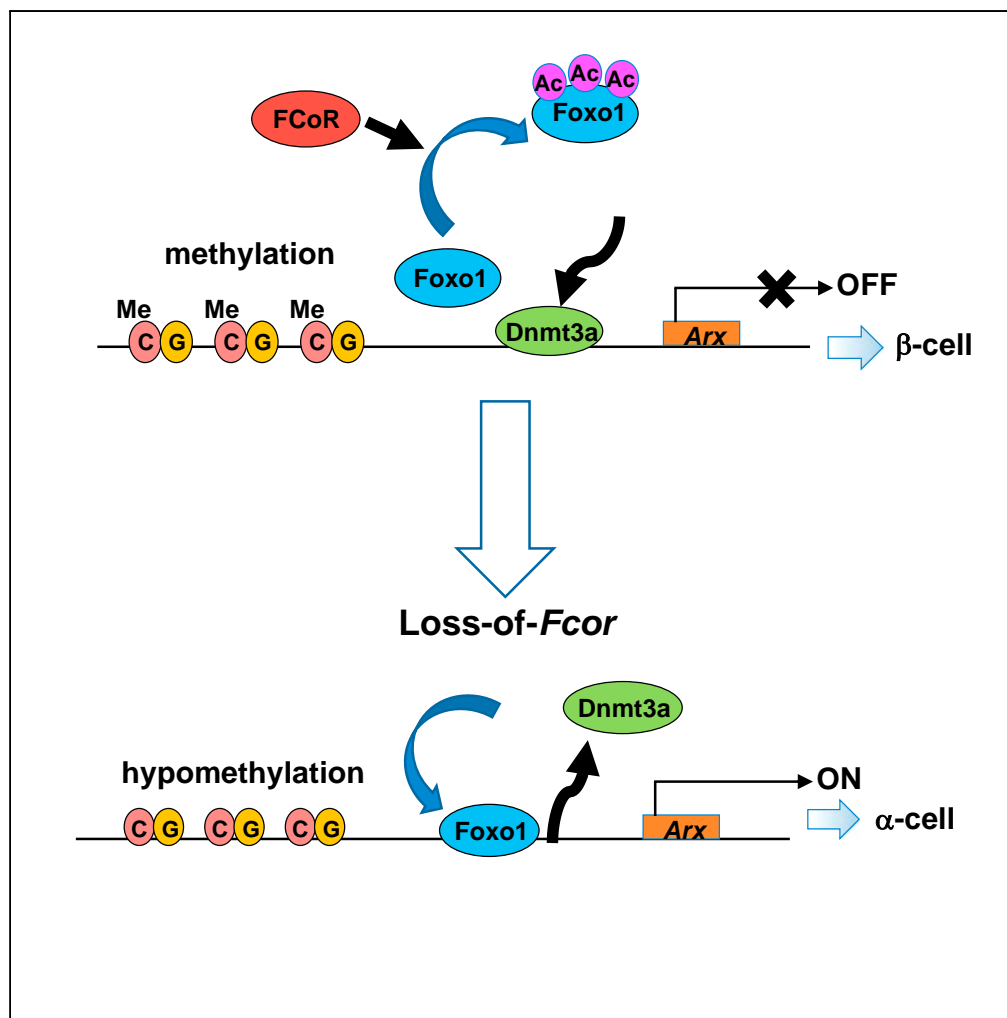**Article**

FCoR-Foxo1 Axis Regulates α-Cell Mass through Repression of *Arx* Expression

Noriko Kodani, Jun Nakae, Masaki Kobayashi, Osamu Kikuchi, Tadahiro Kitamura, Hiroshi Itoh

nakaejun5330@iuhw.ac.jp

HIGHLIGHTS

FCoR increases DNA methylation of *Arx* promoter and decreases *Arx* expression

Loss-of-*Fcor* increases conversion from β- to α-cells

FCoR acetylates and inhibits Foxo1 in pancreatic β-cells

Inactivation of Foxo1 facilitates recruitment of Dnmt3a to *Arx* promoter

Article

FCoR-Foxo1 Axis Regulates α-Cell Mass through Repression of *Arx* Expression

Noriko Kodani,[1] Jun Nakae,[2,4,*] Masaki Kobayashi,[3] Osamu Kikuchi,[3] Tadahiro Kitamura,[3] and Hiroshi Itoh[1]

SUMMARY

Pancreatic endocrine cell development into differentiated α- and β-cells is highly regulated and involves multiple transcription factors. However, the mechanisms behind the determination of α- and β-cell masses remains unclear. We previously identified Foxo1 CoRepressor (FCoR), which inhibits Foxo1 by acetylation. Here we demonstrate that *Fcor*-knockout mice (*FcorKO*) exhibit significantly increased α-cell mass, expression of the master α-cell regulatory transcription factor *Aristaless-related homeobox* (*Arx*), which can be normalized by β-cell-specific FCoR overexpression (*FcorKO-βFcor*), and exhibit β-to-α-cell conversion. Compared with *FcorKO*, β-cell-specific *Foxo1* knockout in the *FcorKO* (DKO) led to decreased *Arx* expression and α-cell mass. Foxo1 binding to *Arx* promoter led to DNA methyltransferase 3a (Dnmt3a) dissociation, *Arx* promoter hypomethylation, and increased *Arx* expression. In contrast, FCoR suppressed *Arx* through Foxo1 inhibition and Dnmt3a recruitment to *Arx* promoter and increased *Arx* promoter methylation. Our findings suggest that the FCoR-Foxo1 axis regulates pancreatic α-cell mass by suppressing *Arx* expression.

INTRODUCTION

Type 2 diabetes results from insulin resistance in peripheral insulin responsive tissues, along with relatively deficient insulin secretion from pancreatic β-cells because of β-cell dysfunction and/or decreased mass. Increased glucagon secretion from α-cells is also found in type 2 diabetes (Dunning and Gerich, 2007; Menge et al., 2011). This hyperglucagonemia may result from decreased insulin-induced inhibition of α-cells or from a relative increase in α-cell mass (Dor and Glaser, 2013). Although apoptosis and proliferation regulate β-cell mass, little is known about the regulation of α-cell mass. "Intra-islet plasticity" has been suggested to be involved in the mechanism for regulating β-cell and other endocrine cell masses (Ziv et al., 2013). Glucagon-expressing α-cells or δ-cells can be converted to β-like cells by near-total genetic ablation of β-cells, forced Pax4 expression, or loss of *Arx* (Thorel et al., 2010) (Collombat et al., 2009) (Courtney et al., 2013). On the other hand, deletion of *Dnmt1*, *Pdx1*, or *Foxo1* converts β-cells to α-cells or other endocrine cells (Dhawan et al., 2011) (Gao et al., 2014) (Talchai et al., 2012b). However, the precise molecular mechanism of conversions among endocrine cell types remains unknown.

Foxo1 may be a key molecule that determines endocrine cell fate at conversion. The loss of *Foxo1* in neurogenin (Ngn)3-positive enteroendocrine progenitors or human fetal pancreatic explants gives rise to insulin-positive cells (Talchai et al., 2012a) (Bouchi et al., 2014). Furthermore, *Foxo1* ablation in pancreatic and endocrine progenitors leads to expanded β-cell mass, whereas *Foxo1* ablation in terminally differentiated β-cells does not have this effect (Talchai and Accili, 2015). These findings indicate that Foxo1 inhibits β-cell differentiation in endocrine progenitor cells. Foxo1 is phosphorylated and inhibited by insulin/IGF-1 through PI3-kinase/Akt and is translocated into the nucleus and activated by oxidative stress (Accili and Arden, 2004). Within the nucleus, Foxo1 is deacetylated and activated by Sirt1 or Hdacs (Accili and Arden, 2004) (Wang et al., 2011) (Mihaylova et al., 2011) (Banks et al., 2011). We recently identified a Foxo1 corepressor (Foxo1 CoRepressor; FCoR) in adipocytes, which acetylates and inhibits Foxo1 activity (Nakae et al., 2012).

Here, we demonstrate that *FcorKO* exhibits significantly increased α-cell mass and expression of the master α-cell regulatory transcription factor *Arx*, which can be normalized by β-cell-specific FCoR overexpression, and that FCoR suppresses *Arx* expression through increased methylation of the *Arx* promoter region by inhibition on Foxo1 activity. In contrast, β-cell-specific *Foxo1* knockout in the *FcorKO* led to decreased *Arx* expression and α-cell mass through loss of Foxo1-induced *Arx* expression. These findings indicate that the FCoR-Foxo1 axis regulates pancreatic α-cell mass via Foxo1 inhibition and suggest new avenues for the development of diabetes therapies.

[1]Division of Nephrology, Endocrinology, and Metabolism, Department of Internal Medicine, Keio University School of Medicine, 35 Shinanomachi, Shinjuku-ku, Tokyo 160-8582, Japan

[2]Department of Physiology, International University of Health and Welfare School of Medicine, Narita 286-8686, Japan

[3]Metabolic Signal Research Center, Institute for Molecular and Cellular Regulation, Gunma University, 3-39-15 Showa-chou, Maebashi, Gunma 371-8512, Japan

[4]Lead Contact

*Correspondence: nakaejun5330@iuhw.ac.jp

https://doi.org/10.1016/j.isci. 2019.100798

RESULTS

FCoR Is Expressed in Pancreatic Islets

FCoR is a Foxo1-binding protein that was originally identified in mouse adipose tissue. Null *FcorKO* exhibits glucose intolerance and insulin resistance (Figures S1A and S1B) (Nakae et al., 2012). Although insulin-resistant mice generally show increased insulin secretion as a result of compensated β-cell hypertrophy, we found that *FcorKO* exhibited decreased glucose-stimulated insulin secretion compared with control (Figure 1A). Additionally, compared with control, *FcorKO* showed significantly increased glucagon secretion at 15 min after glucose stimulation and in response to L-arginine (Figures 1B and 1C).

We next isolated islets and examined their insulin and glucagon secretion in response to glucose or L-arginine. Compared with control islets, islets from *FcorKO* exhibited significantly lower insulin secretion upon stimulation with glucose, whereas insulin secretion in response to L-arginine was similar in islets from *FcorKO* and control (Figure 1D), suggesting decreased glucose sensing and/or normal insulin secretion after depolarization. However, real-time PCR revealed that expression levels of *Slc2a2* and *Gck* in isolated islets of *FcorKO* were similar to those of control (Figure S1C) and the insulin content of *FcorKO* islets was similar to that of control islets (Figure S1D). Therefore, as far as we investigated, we could not reveal the mechanism by which islets from *FcorKO* have the insensitivity to glucose. Additionally, glucagon secretion after stimulation with glucose was significantly greater in *FcorKO* islets compared with control islets (Figure 1E). These data suggested that the dysfunction of insulin and glucagon secretion in *FcorKO* was pancreatic endocrine cell-intrinsic.

In pancreatic tissue from C57Bl6J mice, we performed immunofluorescence analyses for FCoR and glucagon or insulin, which revealed FCoR expression in both α- and β-cells, although FCoR expression in postnatal α-cells was limited (Figure 1F). FCoR moves from cytosol to nucleus through phosphorylation by protein kinase A (PKA) and binds to and acetylates Foxo1 both in cytosol and nucleus (Nakae et al., 2012). On the other hand, the acetylation status of Foxo1 has been known to change intracellular and/or intranuclear localization. Furthermore, deacetylation of Foxo1 by Sirtuins overrides the phosphorylation-dependent nuclear exclusion of Foxo1 caused by growth factors and causes nuclear translocation of Foxo1, leading to activation of Foxo1 (Frescas et al., 2005). Acetylation of Foxo1 by FCoR in cytosol may also inhibit Foxo1 owing to cytosolic retention. Therefore, FCoRs may be active both in cytosol and nucleus. Additionally, to investigate whether FCoR expression in islets was modulated at insulin-resistant state, we examined FCoR protein expression in islets of mice fed a high-fat diet (HFD) or of *Lepr*$^{db/db}$. An HFD led to decreased FCoR expression in the islets of C57Bl6J mice (Figure 1G) and FCoR expression was also decreased in *Lepr*$^{db/db}$ (Figure 1H). These data suggested that FCoR may play some physiological roles in islets.

Furthermore, immunofluorescence analyses in mouse embryos demonstrated co-localization of FCoR in both insulin- and glucagon-positive cells starting at embryonic day 14.5 (Figures 1I–1K). Although FCoR expression was increased in insulin-positive cells after embryonic day 16.5 and was in almost all insulin-positive cells after embryonic day 18.5, FCoR expression was decreased in glucagon-positive cells after embryonic day 14.5 (Figures 1I–1K). At embryonic day 14.5, FCoR was expressed in most of the glucagon-positive cells, which later decreased. In contrast, after embryonic day 18.5, all insulin-positive cells expressed FCoR (Figure 1K). FCoR was not co-localized within neurogenin 3 (Ngn3)-positive cells during these embryonic stages (data not shown). Foxo1 was expressed mainly in glucagon-positive cells until embryonic day 17.5. Furthermore, after that, Foxo1 was expressed in insulin-positive cells rather than in glucagon-positive cells (Figures S1E–S1H). These data suggest that FCoR expression occurs just after the development of pancreatic endocrine progenitors (Puri and Hebrok, 2010) and may be related to the development of pancreatic endocrine cell differentiation and that FCoR and Foxo1 may be co-localized in glucagon-positive cells before embryonic day 15.5.

Fcor Ablation Increases Arx Expression and α-Cell Mass

To investigate the effects of *Fcor* deletion on pancreatic islets, we examined α-cell and β-cell masses. Immunofluorescence analyses revealed significantly increased α-cell mass in *FcorKO* compared with control, with no significant difference in β-cell mass (Figures 2A–2C). The sizes did not differ between control and *FcorKO* islets (data not shown). The architecture of islets from *FcorKO* was normal, which indicated peripheral localization of α-cells (Figure 2A). In contrast, transgenic mice overexpressing FCoR specifically in β-cells in a *FcorKO* genetic background (*FcorKO-βFcor*, developed using *RIP-Cre* transgenic mice;
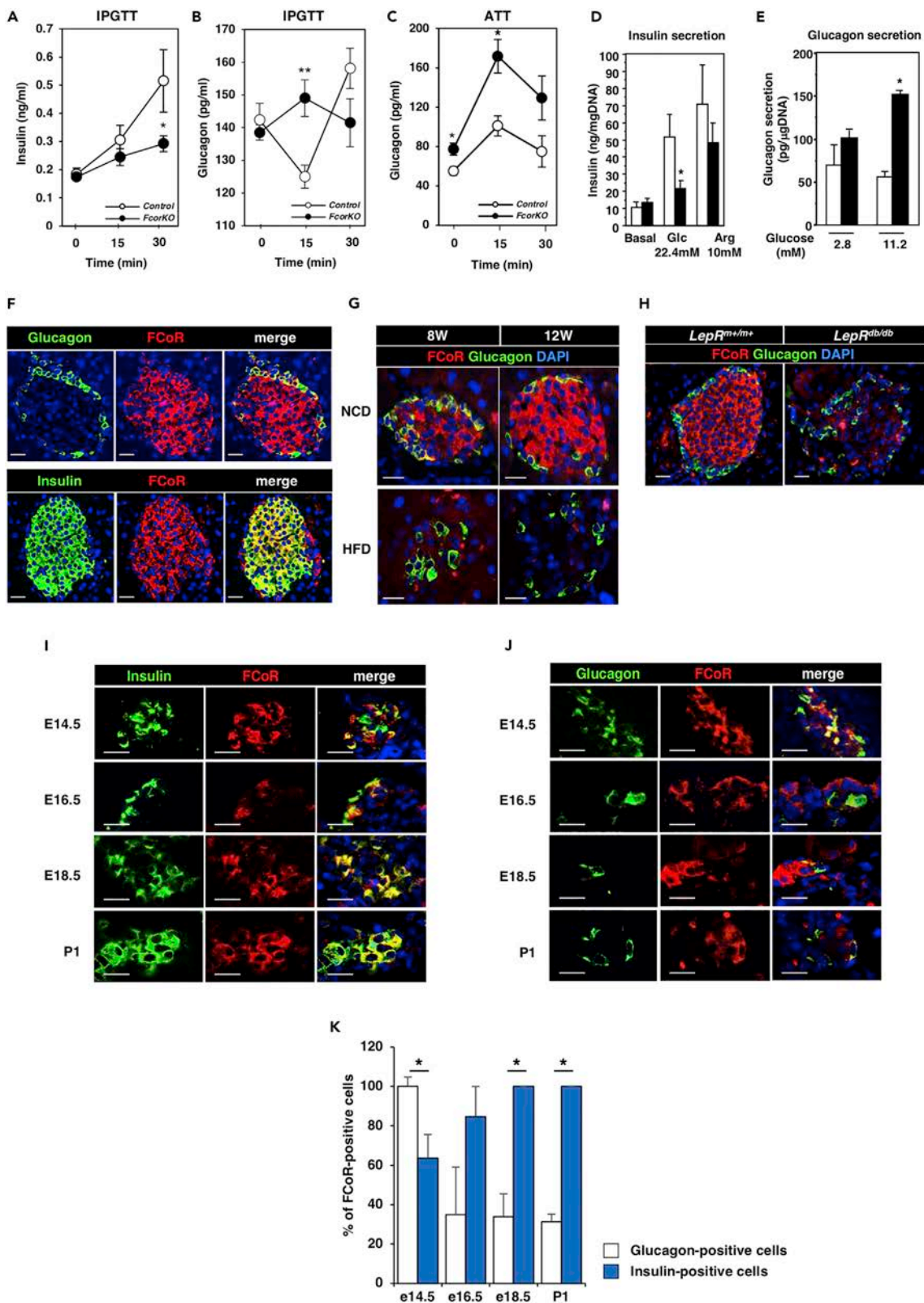
Figure 1. FCoR Is Expressed in Pancreatic Islets

(A) Insulin secretion during an intraperitoneal glucose tolerance test (IPGTT) in control (open circle, $n = 7$) and *FcorKO* (closed circle, $n = 10$). Data represent means ± SEM. *$p < 0.05$ by two-way ANOVA with Fisher's test.

(B and C) Glucagon secretion during the IPGTT (control, $n = 11$; *FcorKO*, $n = 15$) (B), and L-arginine tolerance test (ATT) (control, $n = 5$; *FcorKO*, $n = 9$) (C). Data represent means ± SEM. *$p < 0.05$ and **$p < 0.005$ by two-way ANOVA with Fisher's test.

(D and E) Insulin (D) and glucagon (E) secretion in response to glucose or L-arginine tolerance tests in islets isolated from WT (white bar, $n = 6$) and *FcorKO* (black bar, $n = 6$). Data represent means ± SEM. *$p < 0.05$ by one-way ANOVA.

(F) Immunofluorescence of pancreatic islets for FCoR and glucagon or FCoR and insulin in islets from the 24-week-old C57Bl6J mouse. Scale bar, 20 μm. DAPI, 4′,6-diamidino-2-phenylindole.

(G and H) Immunofluorescence of pancreatic islets for FCoR and glucagon from mice fed a normal chow and a high-fat diet (G), and from $Lepr^{m+/m+}$ and $Lepr^{db/db}$ (H). Scale bar, 20 μm.

(I and J) Representative images of pancreatic islets for FCoR and insulin (I) or FCoR and glucagon (J) from embryos at embryonic days 14.5 (E14.5), 16.5 (E16.5), and 18.5 (E18.5), and postnatal day 1 (P1). Scale bar, 20 μm.

(K) The percentage of embryonic cells stained with FCoR among glucagon- or insulin-positive cells at embryonic day 14.5 (percentage of FCoR-stained cells/glucagon-positive cells versus FCoR-stained cells/insulin-positive cells $100 ± 4.76$: $63.6 ± 12.0$, $n = 3$; 42 glucagon-positive cells, 193 insulin-positive cells counted, consistent for all comparisons), embryonic day 16.5 ($34.8 ± 24.3$: $84.8 ± 15.2$, $n = 3$; 40 glucagon-positive cells, 36 insulin-positive cells), embryonic day 18.5 ($34 ± 11.5$: $100 ± 0$, $n = 3$; 71 glucagon-positive cells, 86 insulin-positive cells counted), and P1 ($31.3 ± 3.86$: $100 ± 0$, $n = 3$; 136 glucagon-positive cells, 78 insulin-positive cells counted). Data represent means ± SEM. *$p < 0.05$ by one-way ANOVA.

Figures S2A–S2D) showed an α-cell mass similar to that of controls (Figures 2A–2C). Furthermore, to investigate the effects of FCoR on α-cell mass, we generated transgenic mice overexpressing α-cell-specific FCoR (*αFcor*) (Figures S2B, S3A, and S3B). Immunofluorescence demonstrated significantly decreased α-cell mass in *αFcor* compared with controls, but β-cell mass in *αFcor* was similar to that of control (Figure S3C). These findings indicated that FCoR plays an important role in regulating α-cell mass.

To investigate the mechanism behind the increased α-cell mass in *FcorKO*, we isolated islets from control, *FcorKO*, and *FcorKO-βFcor* and measured the expression levels of α-cell-specific genes. Real-time PCR revealed significantly increased expression of α-cell-specific genes (*Gcg*, *Arx*, and *Mafb*) in *FcorKO* compared with control (Figure 2D). In contrast, *Gcg*, *Arx*, and *Mafb* expressions in islets isolated from *FcorKO-βFcor* were similar to control levels (Figure 2D). Furthermore, *Arx* expression was significantly decreased in *αFcor* (Figure S3D). Moreover, immunofluorescence analyses of pancreas from 20- to 24-week-old adult mice revealed that the nuclear Arx protein was less detectable in α-cells from control mice, whereas nuclear Arx expression was present in most α-cells in *FcorKO* (Figures 2E and 2F). These data suggested that FCoR suppressed *Arx* expression in islets and that *Fcor* knockout led to increased Arx expression in islets.

To investigate whether the increased α-cell mass observed in *FcorKO* resulted from increased *Arx* expression during the embryonic stage, we performed immunofluorescence analysis with anti-Arx antibody. During pancreatic development, the master regulator of pancreatic islet differentiation and regeneration, Ngn3, was expressed in endocrine precursor cells starting at embryonic day 9.5 (Rukstalis and Habener, 2009). Subsequently, the Ngn3-positive cells that were also Arx positive differentiated into α-cells (Collombat et al., 2006). Immunofluorescence analysis revealed significantly more Arx-positive cells in *FcorKO* compared with controls on embryonic day 15.5 (Figures 2G and 2H). At embryonic day 15.5, there were no significant differences in numbers of insulin-positive cells between control and *FcorKO* (Figure 2I). Therefore, we counted the numbers of Arx-positive cells corrected by the numbers of insulin-positive cells counted. From embryonic day 16.5 to birth, endocrine cell lineages organize into clusters to form the islets (Habener et al., 2005; Rukstalis and Habener, 2009). Immunofluorescence of the fetal pancreas at embryonic day 17.5 revealed significantly more glucagon-positive cells in *FcorKO* compared with control (Figures 2J–2L). These results suggested that FCoR regulated *Arx* expression from the embryonic stage and controlled α-cell mass.

During development of pancreatic endocrine cells, a complex network of transcription factors, including Arx and Pax4, drives endocrine precursor cells toward the different endocrine cell fate. These two transcription factors mutually inhibit the other's transcription and display antagonistic activities for proper endocrine cell lineage allocation (Collombat et al., 2005). Indeed, expression levels of the β-cell-specific gene *Pax4* in islets isolated from *FcorKO* were significantly decreased compared with control and *FcorKO-βFcor* (Figure 2M). However, mature β-cell-specific marker genes (*Pdx1*, *Mafa*, *Neurod*, and *Unc3*) expression levels in islets from *FcorKO* were significantly increased compared with control and *FcorKO-βFcor* cells (Figure 2M).
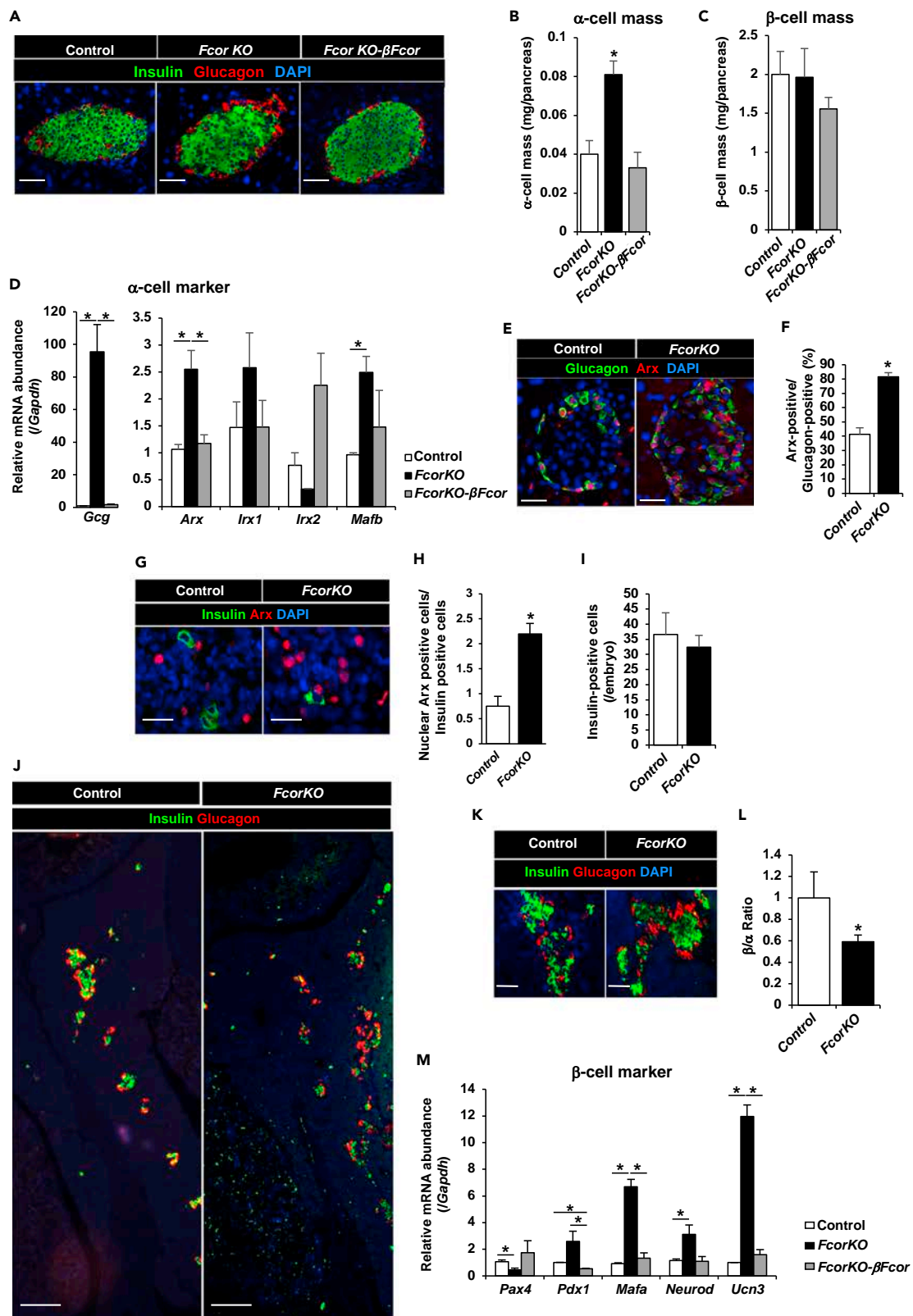
Figure 2. FCoR Regulates *Arx* Expression and α-Cell Mass

(A) Immunofluorescence of insulin and glucagon in islets from control, *FcorKO*, and *FcorKO-βFcor* at age 24 weeks. Scale bar, 50 μm.

(B and C) Quantification of α-cell (B) and β-cell masses (C) in control (n = 7 mice; 230 islets measured), *FcorKO* (n = 5 mice; 220 islets measured), and *FcorKO-βFcor* (n = 3 mice; 80 islets measured). Four sections ~200 μm apart were covered systematically by accumulating images from non-overlapping fields for whole pancreas sections. Data represent means ± SEM. *p < 0.05 by one-way ANOVA.

(D) Expression levels of α-cell marker genes in islets isolated from control (white bar) (n = 4), *FcorKO* (black bar) (n = 4), and *FcorKO-βFcor* (gray bar) (n = 4) at the age of 20–24 weeks. Data represent means ± SEM. *p < 0.05 by one-way ANOVA.

(E and F) Representative images of Arx and glucagon immunostaining of islets from control and *FcorKO* at age 20 weeks (E), and the percentages of Arx-positive cells among glucagon-positive cells (F). We have calculated Arx-positive and glucagon-positive cells in 3–5 sections from each 5 mice. Data represent means ± SEM. *p < 0.05 by one-way ANOVA. Scale bar, 50 μm.

(G and H) Representative image of immunofluorescence for Arx and insulin in fetal pancreas on embryonic day 15.5 (G), and the ratio of numbers of nuclear Arx-positive cells and of insulin-positive cells per field; control, 0.75 ± 0.20, n = 5 mice, 90 Arx-positive cells and 166 insulin-positive cells counted; *FcorKO*, 2.20 ± 0.21; n = 5 mice, 261 Arx-positive cells and 114 insulin-positive cells counted (H). Data represent means ± SEM. *p < 0.05 by one-way ANOVA. Scale bar, 20 μm.

(I) The numbers of insulin-positive cells in each 2 section from fetal pancreases of control (n = 5) and *FcorKO* (n = 5) at embryonic day 15.5. Data represent means ± SEM.

(J) Representative immunofluorescence images of insulin and glucagon staining in fetal pancreas of control and *FcorKO* at embryonic day 17.5. Scale bar, 200 μm.

(K and L) The α-cell and β-cell numbers of control and *FcorKO* at embryonic day 17.5. Representative image (K) and β- to α-cell ratio are (L): control, 1 ± 0.24, n = 3, 3 sections for each mouse was measured; *FcorKO*, 0.59 ± 0.06, n = 3 mice, 3–4 sections for each mouse was measured. Data represent means ± SEM. *p < 0.05 by one-way ANOVA. Scale bar, 50 μm.

(M) Expression levels of β-cell marker genes in islets isolated from control (white bar) (n = 4), *FcorKO* (black bar) (n = 4), and *FcorKO-βFcor* (gray bar) (n = 4) at the age of 20–24 weeks. Data represent means ± SEM. *p < 0.05 by one-way ANOVA.

FCoR Regulates Arx Expression in Cell Lines

We next investigated the direct effects of FCoR on *Arx* expression by infecting the α-cell-line αTC1 cells with adenoviruses encoding LacZ or FLAG-tagged FCoR and examining the cellular expression of *Arx*. Real-time PCR analysis revealed that *Fcor* expression level in αTC1 cells was significantly lower than in the β-cell line MIN6 (Figure S4A). FCoR overexpression in αTC1 cells significantly and dose-dependently decreased *Arx* expression (Figure S4B). In contrast, expression levels of the β-cell-specific marker genes, *Pax4*, *Mafa*, and *Ins1*, were significantly increased in FCoR-infected cells compared with LacZ-infected cells, although expression levels of the α-cell-specific marker genes *Mafb* and *Gcg* were unaffected (Figure S4C). Furthermore, we examined the effects of FCoR knockdown on *Arx* expression in MIN6 cells. *Arx* expression was significantly increased in MIN6 cells infected with adenovirus encoding short hairpin RNA (shRNA) targeting FCoR (which showed 85% knockdown of endogenous FCoR), compared with that in MIN6 cells infected with adenovirus encoding SCR-shRNA (Figure S4D). In contrast, *Pax4* and *Mafa* expression levels were significantly decreased in FCoR-knockdown cells compared with those in SCR shRNA-infected cells. Expression levels of α-cell-specific marker genes *Mafb* and *Gcg* tended to be increased in FCoR-knock-down MIN6 cells but not statistically significantly (Figure S4E). These data indicated that FCoR suppresses *Arx* and increases *Pax4* expression.

Fcor Ablation Causes β-to-α-Cell Conversion

To examine whether the increased α-cell mass in *FcorKO* resulted from increased conversion from β-cells to α-cells, we performed a double immunostaining of EGFP and glucagon using control or *FcorKO* with the transgene *RIP-Cre: EGFP* (Figure S5). The confocal microscopy analyses demonstrated that EGFP was stained exclusively in the β-cell area in control mice. One EGFP-positive cell (0.17%) was detected among 574 glucagon-positive cells of 38 islets from three control mice. In contrast, *FcorKO* exhibited cells co-stained with EGFP and glucagon, indicating conversion from β-cells to α-cells. A total of 90 EGFP-positive cells (2.47%) were detected among 3,644 glucagon-positive cells of 195 islets from five *FcorKO* mice (Figures 3A and 3B). Moreover, a 3D reconstruction of z stack images of pancreas from a 5-μm section also identified EGFP- and glucagon-double-positive cells (Figure 3C). Furthermore, double immunostaining of insulin and glucagon revealed a significantly increased number of double-positive cells in islet of *FcorKO* compared with control (Figures 3D and 3E). The presence of these cells indicates conversion from β-cells to α-cells and bihormonal and immature cells.

To explore the alternative mechanism that α-cells may undergo expansion, we performed Ki67-staining in glucagon-positive cells from control and *FcorKO* mice at the ages of e15.5, e17.5, and adulthood. However, we detected no recognizable differences in glucagon-positive cells between control and FcorKO (Figure S6). These data indicate that α-cell expansion in *FcorKO* does not result from increased
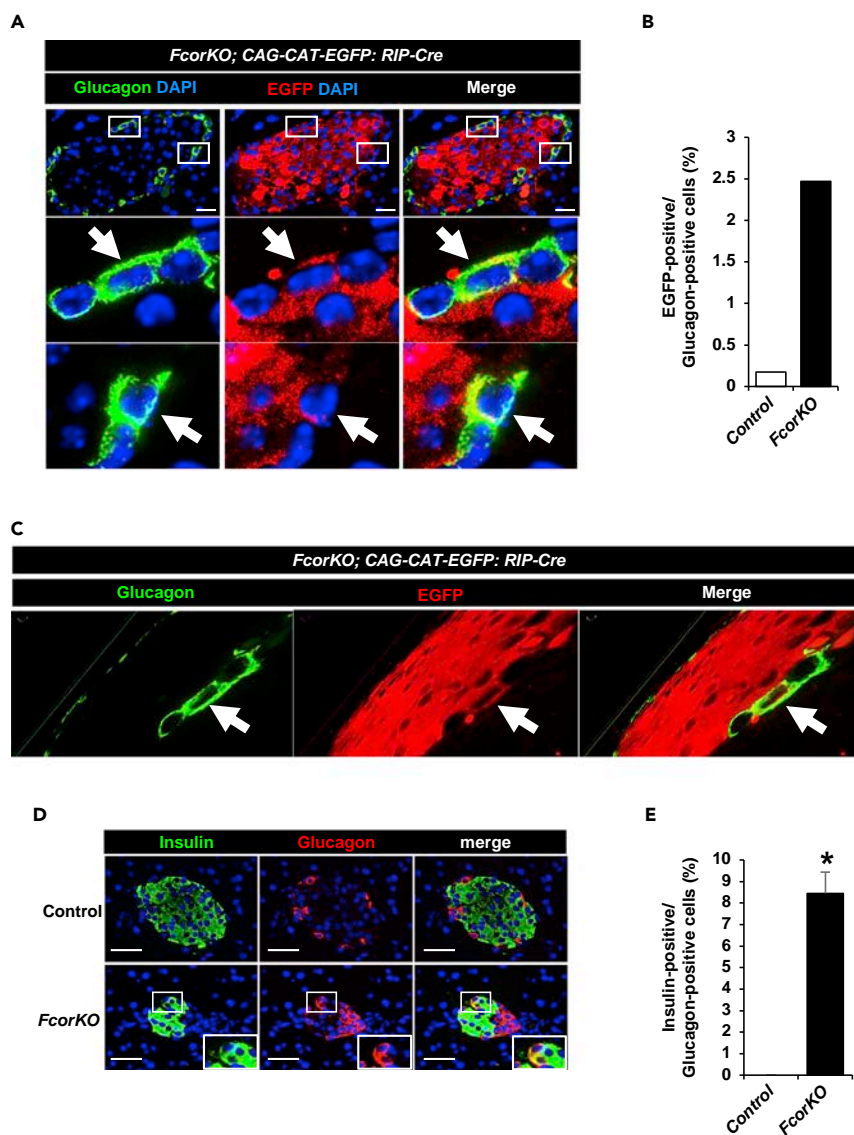
Figure 3. *Fcor* Ablation Causes β-to-α-Cell Conversion

(A) β-Cell lineage tracing of control (*CAG-CAT-EGFP:RIP-Cre*) and *FcorKO* (*FcorKO:CAG-CAT-EGFP: RIP-Cre*) at age 24 weeks. The sections were examined with a confocal microscope (Olympus Fluoview FV3000). White arrows indicate EGFP- and glucagon-double-positive cells. Scale bar, 20 μm.

(B) The percentage of EGFP-positive cells among glucagon-positive cells in islets from control and *FcorKO*. In control mice, one EGFP-positive cell (0.17%) was detected among 574 glucagon-positive cells of 38 islets from three control mice. In contrast, 90 EGFP-positive cells (2.47%) were detected among 3,644 glucagon-positive cells of 195 islets from five *FcorKO*.

(C) Z sectioning and 3D reconstruction of a 5-μm section of pancreas from *FcorKO:CAG-CAT-EGFP: RIP-Cre* shows a glucagon- and EGFP-double-positive cell.

(D and E) Representative image of immunofluorescence for insulin and glucagon in pancreas at the age of 24 weeks (D), and the percentage of numbers of insulin-positive cells among glucagon-positive cells (E); control, 2 sections from each mouse (n = 3), 0 insulin-positive cells among 46 islets counted; *FcorKO*, 2 sections from each mouse (n = 3), 12 insulin-positive cells among 77 islets counted. Data represent means ± SEM. *p < 0.05 by one-way ANOVA. Scale bar, 50 μm.

proliferation of α-cells. Furthermore, to investigate whether β-cells proliferate more to compensate the loss of β-cells due to β-to-α-cell conversion, we performed double staining of insulin and Ki67 of islets using the same samples. However, there were also no significant differences in insulin-positive cells (data not shown). These indicate that there is no increased proliferation of β-cell in *FcorKO* mice. Moreover, no

Ngn3-positive cells were present in islets isolated from adult *FcorKO* mice, excluding the possibility that the converted cells were not attributable to dedifferentiated cells (data not shown). These results suggested that the conversion from β- to α-cells contributed to increased α-cell mass in *FcorKO*.

FCoR Is a Regulator of Foxo1 Activity in Islets

FCoR enhances the acetylation of Foxo1 and Foxo3, thus inhibiting their transcriptional activity (Nakae et al., 2012). Indeed, compared with control, islets isolated from *FcorKO* showed significantly greater deacetylation of transduced ADA-Foxo1, which was a constitutively nuclear mutant Foxo1 (Nakae et al., 2001), and stronger binding to Sirt1 (Figure 4A). Furthermore, immunofluorescence analyses revealed nuclear localization of endogenous Foxo1 in islets from *FcorKO*, in both α-cells and non-α-cells (Figure 4B), suggesting that Foxo1 may have been active. In addition, western blotting showed that endogenous Foxo1 protein expression level was significantly decreased in islets isolated from *FcorKO* compared with controls (Figure 4C), consistent with previous findings demonstrating that deacetylated Foxo1 is quickly ubiquitinated and degraded (Kitamura et al., 2005). These data indicate that FCoR is one of the regulators of Foxo1 acetylation and intracellular localization in islets.

If Foxo1 activation in islets mediates the phenotypes of *FcorKO*, including *Arx* expression and α-cell mass, then additional knockout of *Foxo1* specifically in β-cells could rescue the *FcorKO* phenotype. To examine this hypothesis, we generated double-knockout mice, β-cell-specific *Foxo1KO (βFoxo1KO)* in the background of *FcorKO (DKO)* (Figure 4D). Real-time PCR of islets isolated from each genotype revealed significantly decreased *Foxo1* expression levels in *βFoxo1KO* and *DKO* mice compared with control and *FcorKO*. *Foxo3* and *Foxo4* expression levels were similar in islets isolated from each genotype, except for increased *Foxo3* expression in *FcorKO* (Figure S7A).

Real-time PCR demonstrated that *Arx* expression level in islets isolated from *DKO* was significantly decreased compared with *FcorKO* and similar to controls. Furthermore, *Arx* expression level in islets isolated from *βFoxo1KO* was significantly lower than from any other genotyped islets (Figure 4E). Furthermore, immunofluorescence analyses also revealed that Arx staining in α-cells of *FcorKO* was more prominent than in control and *DKOs*. In contrast, Arx staining in α-cells from *βFoxo1KO* was difficult to be detected (Figures S7B and S7C). These data indicate that increased expression of *Arx* in islets from *FcorKO* results from Foxo1 activation in islets and that Foxo1 may have an important role in the regulation of *Arx* expression. Furthermore, immunofluorescence analyses revealed that the α-cell mass in *DKO* was significantly decreased compared with that in *FcorKO*, although it was still significantly increased compared with controls (Figure 4F). The groups did not significantly differ in β-cell mass or number of islets (Figure 4G). These data indicate that increased *Arx* expression and α-cell mass with the *FcorKO* genotypes results from Foxo1 activation.

Arx Is a Target Gene of Foxo1

As described above, loss of *Foxo1* in β-cells significantly decreased *Arx* expression compared with control, *FcorKO*, and *DKO*, although it did not affect the architecture of islets (Figures 4E–4G). These data led us to speculate that Foxo1 itself may affect endogenous *Arx* expression. To investigate the influence of Foxo1 on endogenous *Arx* expression, we infected MIN6 cells with adenovirus encoding constitutively nuclear HA-ADA Foxo1 (Nakae et al., 2001). Real-time PCR demonstrated that *Arx* expression was significantly increased compared with LacZ-infected control cells (Figure 5A). These data indicated that Foxo1 induced *Arx* expression. The murine *Arx* gene contains a conserved forkhead responsive element (FRE) in its promoter region (Figures S8A and S8B). ChIP assay results confirmed that constitutively nuclear Foxo1 mutant (HA-ADA) bound to the *Arx* promoter region, including FRE, in MIN6 cells (Figure 5B).

To assess whether Foxo1 directly induced *Arx* expression, we performed the *Arx* promoter assay in MIN6 cells using *Arx* promoter regions of various lengths. We found that FLAG-tagged constitutively nuclear mutant Foxo1 (FLAG-3AFoxo1) (Nakae et al., 2006) significantly increased the luciferase activity in the FRE-containing *Arx* promoter (Figure 5C) but did not do so in the truncated *Arx* promoter lacking FRE or in the *Arx* promoter with mutated FRE (Figure 5C). Moreover, site-directed mutagenesis of FRE in the *Arx* promoter completely abolished Foxo1-induced luciferase activity (Figure 5C).

We next conducted an electrophoretic mobility shift assay (EMSA) to further examine the ability of this putative FRE to bind Foxo1. A cMyc-tagged Foxo1 caused significant retardation of the FRE DNA (Figure 5D,
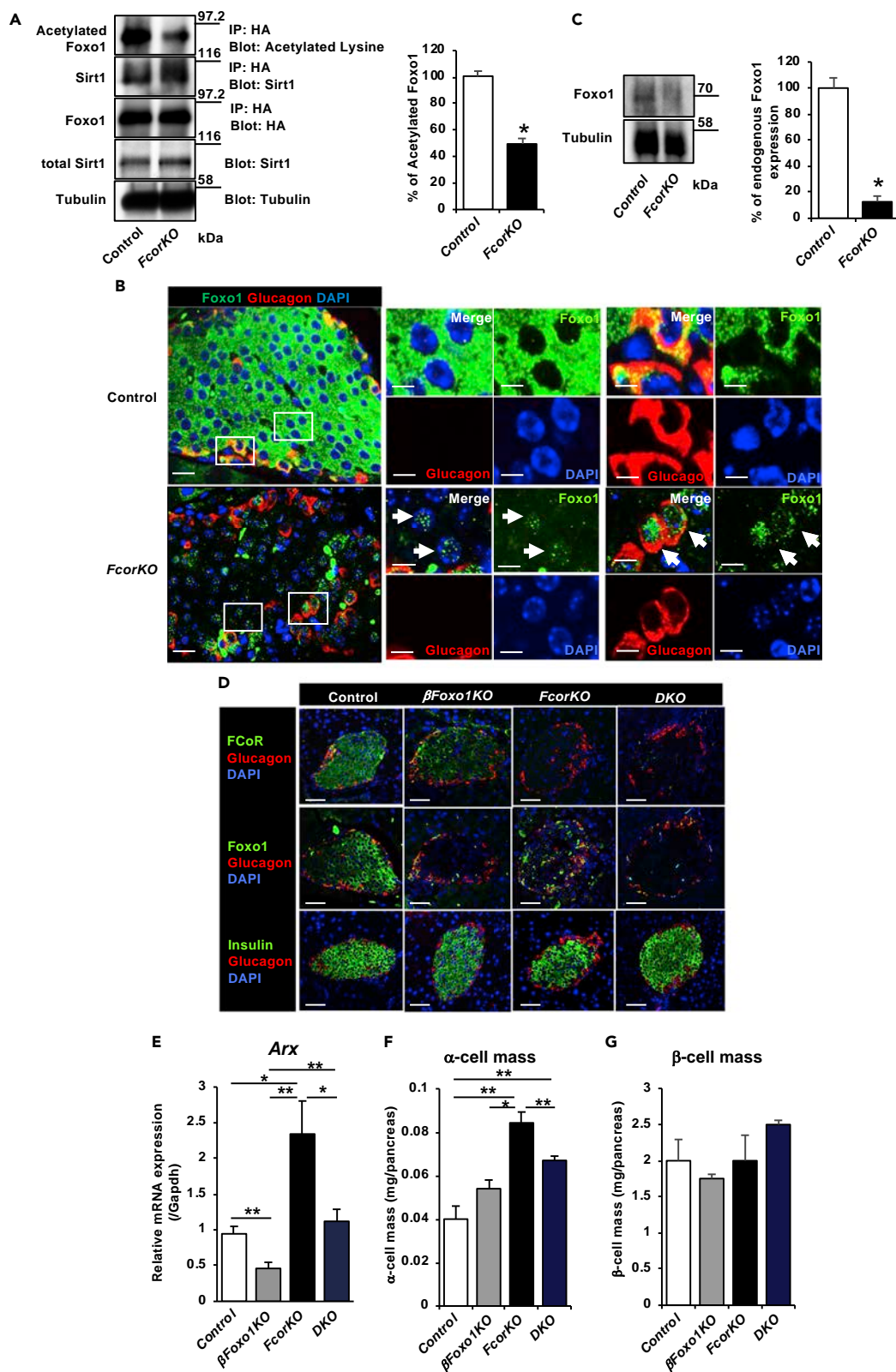
Figure 4. FCoR-Foxo1 Axis Regulates *Arx* Expression and α-Cell Mass

(A) Transduced Foxo1 deacetylation in islets isolated from *FcorKO*. Islets isolated from control and *FcorKO* were transduced with adenoviruses encoding HA-tagged ADA-Foxo1 and harvested at 36 h after transduction. Cell lysates were immunoprecipitated with anti-HA and blotted with the indicated antibodies. The left panel indicates representative western blotting, and the right panel indicates the quantitative analysis of acetylated HA-tagged ADA Foxo1 in islets. The intensity of each band was measured using NIH ImageJ, and the intensity of band of acetylated HA-tagged ADA Foxo1 was corrected by total HA-tagged ADA Foxo1 and calculated as the percentage of control. Data represent means ± SEM from three independent experiments. *p < 0.05 by one-way ANOVA.

(B) Representative immunofluorescence of nuclear localization of endogenous Foxo1 and glucagon-positive cells in islets from 16-week-old control and *FcorKO*. Scale bar, 20 μm. Insets represent endogenous nuclear Foxo1 and glucagon-negative (left panel) or glucagon-positive cells (right panel). Arrows indicate endogenous nuclear Foxo1-positive cells. Scale bar, 20 μm.

(C) Endogenous Foxo1 protein expression level was decreased in islets isolated from *FcorKO* compared with control. The top panel indicates representative western blotting, and the bottom panel indicates the quantitative analysis of endogenous Foxo1 in islets. The intensity of each band was measured using NIH ImageJ, and the intensity of band of endogenous Foxo1 was corrected by tubulin and calculated as the percentage of control. Data represent means ± SEM from three independent experiments. *p < 0.05 by one-way ANOVA.

(D) Representative double immunofluorescence of islets from 24-week-old controls and from *FcorKO*, *DKO*, and *βFoxo1KO* using anti-glucagon and anti-FCoR, anti-Foxo1, or anti-insulin antibodies. Scale bar, 50 μm.

(E) *Arx* expression level in islets isolated from 20- to 24-week-old controls (n = 4) and from *β Foxo1KO* (n = 4), *FcorKO* (n = 4), and *DKO* (n = 4). Data represent means ± SEM from three independent experiments. *p < 0.05 and **p < 0.005 by one-way ANOVA.

(F and G) Quantification of α-cell (F) and β-cell masses (G) in 20- to 24-week-old control (n = 3 mice; 70 islets measured), *βFoxo1KO* (n = 3; 61 islets measured), *FcorKO* (n = 4 mice; 102 islets measured), and *DKO* (n = 4; 98 islets measured). Data represent means ± SEM. *p < 0.05 and **p < 0.005 by one-way ANOVA.

lane 4), and inclusion of the anti-cMyc antibody resulted in a supershifted DNA band (Figure 5D, lane 5). As a control, we performed the same EMSA using a mutant DNA containing five base substitutions within the FRE motif. Alteration of this consensus FRE motif abrogated its ability to bind Foxo1 (Figure 5D, lane 7). We incubated nuclear extracts from cells expressing cMyc-tagged Foxo1 with a probe encoding the 31-base pair FRE DNA sequence, which yielded a slower complex that was competed out by excess cold probe but not mutant probe (Figure 5E). These data indicated that Foxo1 directly induced *Arx* and that *Arx* was a target gene of Foxo1.

FCoR Induces DNA Methylation of the *Arx* Promoter Region

Epigenetic regulation in the *Arx* promoter region controls *Arx* expression. The *Arx* promoter region is methylated, and its expression is suppressed in β-cells, whereas in α-cells, this promoter is hypomethylated and *Arx* is expressed. One well-studied methylation locus is the CpG-rich UR2 region located upstream of the transcription start site, from −2,103 to around −1,992 nt (Papizan et al., 2011). Bisulfite sequencing analysis of the *Arx* upstream promoter region revealed that a vast majority of CpG dinucleotides in the UR2 region were methylated in MIN6 cells, but hypomethylated in αTC1 cells (Figure S9A), consistent with previous findings (Dhawan et al., 2011). Intrinsic FCoR expression level was low in αTC1 cells and high in MIN6 cells (Figure S4A). Therefore, to investigate the effects of FCoR on *Arx* methylation, we over-expressed FCoR in αTC1 cells (through infection with adenovirus encoding FLAG-FCoR) and we knocked down Fcor in MIN6 cells (through infection with adenovirus encoding FCoR-targeting shRNA). Bisulfite sequencing of the UR2 region revealed that methylation in the UR2 locus was significantly increased in FCoR-overexpressing αTC1 cells (Figure 6A) and was significantly decreased in FCoR-knockdown MIN6 cells (Figure 6B). Methylation of the CpG-rich UR2 region enables binding of methyl CpG binding protein 2 (MeCP2) to this area (Dhawan et al., 2011). We next conducted a chromatin immunoprecipitation (ChIP) assay in αTC1 cells infected with adenovirus encoding FLAG-FCoR or LacZ. The results revealed that MeCP2 bound to the UR2 regulatory region of the *Arx* promoter, whereas we observed no binding in αTC1 cells infected with adenovirus encoding LacZ (Figure S9B).

DNA methylation requires conducive histone modifications at target genes (Martin and Zhang, 2007). For this reason, we explored histone modification associated with *Arx* in αTC1 cells overexpressing FCoR. A ChIP assay using anti-H3K4 trimethylation (H3K4me3) antibody, which is implicated in activation of transcription (Kouzarides, 2007), in αTC1 cells overexpressing FCoR showed significantly low levels of H3K4me3 at the UR2 region of *Arx* promoter compared with control αTC1 cells. This result indicates that FCoR overexpression induces a repressed chromatin state of the UR2 region of *Arx* promoter (Figure S9C). Furthermore, a ChIP assay using anti-H3K9 trimethylation (H3K9me3) showed significantly low levels of this histone modification at the *Arx* locus in *Fcor*-knockdown MIN6 cells compared with SCR-MIN6 cells (Figure S9D). Because H3K9me3 is implicated in the silencing of euchromatic genes as well as in forming silent heterochromatin, which is transcriptionally inert (Berger, 2007), a low level of H3K9me3 in the *Arx* UR2 region of *Fcor*-knockdown MIN6 cells indicates an open chromatin state and active transcription of *Arx*.
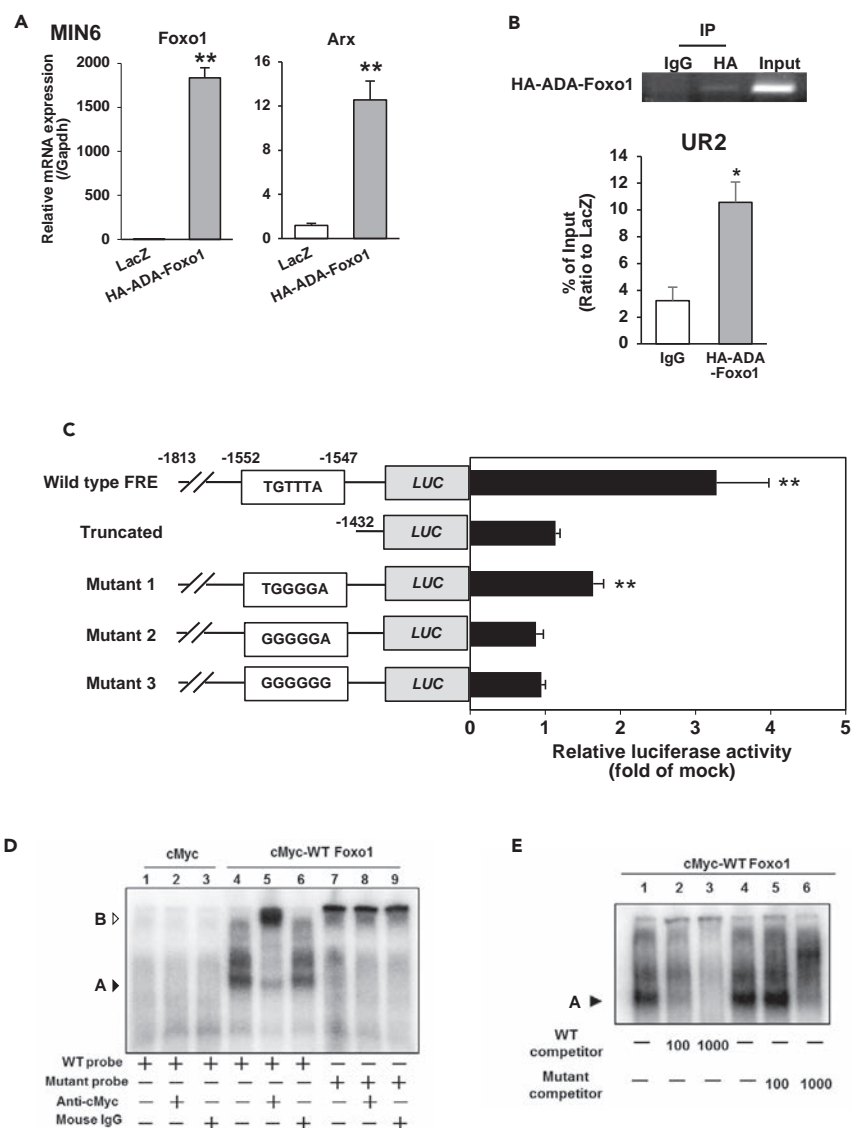
Figure 5. *Arx* Is a Target Gene of Foxo1

(A) Foxo1 induces *Arx* expression in MIN6 cells. MIN6 cells were transduced with adenoviruses encoding LacZ (white bar) or HA-ADA-Foxo1 (gray bar) and harvested at 48 h after transduction. Data represent means ± SEM from three independent experiments. *p < 0.05 and **p < 0.005 by one-way ANOVA.

(B) ChIP assay of MIN6 cells transduced with adenoviruses encoding LacZ (white bar) or HA-ADA-Foxo1 (gray bar) and harvested at 48 h after transduction. Samples were subjected to immunoprecipitation with anti-HA, followed by PCR amplification of the UR2 region. Data represent means ± SEM from three independent experiments. *p < 0.05 by one-way ANOVA.

(C) Effect of Foxo1 on *Arx* promoter activity. Data were obtained from 10 experiments and are shown as mean ± SEM of the fold-change from mock vector-transfected activity. Data represent means ± SEM from three independent experiments. **p < 0.005 by one-way ANOVA.

(D) EMSA of Foxo1 binding to DNA. The DNA probe was a DNA fragment of 31 base pairs covering the consensus Foxo1-binding site (−1552/−1547 nt) of the mouse *Arx* promoter (lanes 1–6). A mutant DNA with an altered Foxo1-binding motif was used as a control (lanes 7–9). The position of the gel-retarded complex is indicated as A and that of the super-shifted complex is indicated as B.

(E) Oligonucleotide probes corresponding to the Foxo1-binding site of the *Arx* promoter were incubated with nuclear extracts in the absence or presence of increasing amounts of unlabeled wild-type (lanes 1–3) or mutant oligonucleotide (lanes 4–6). The position of the gel-retarded complex is indicated as A.
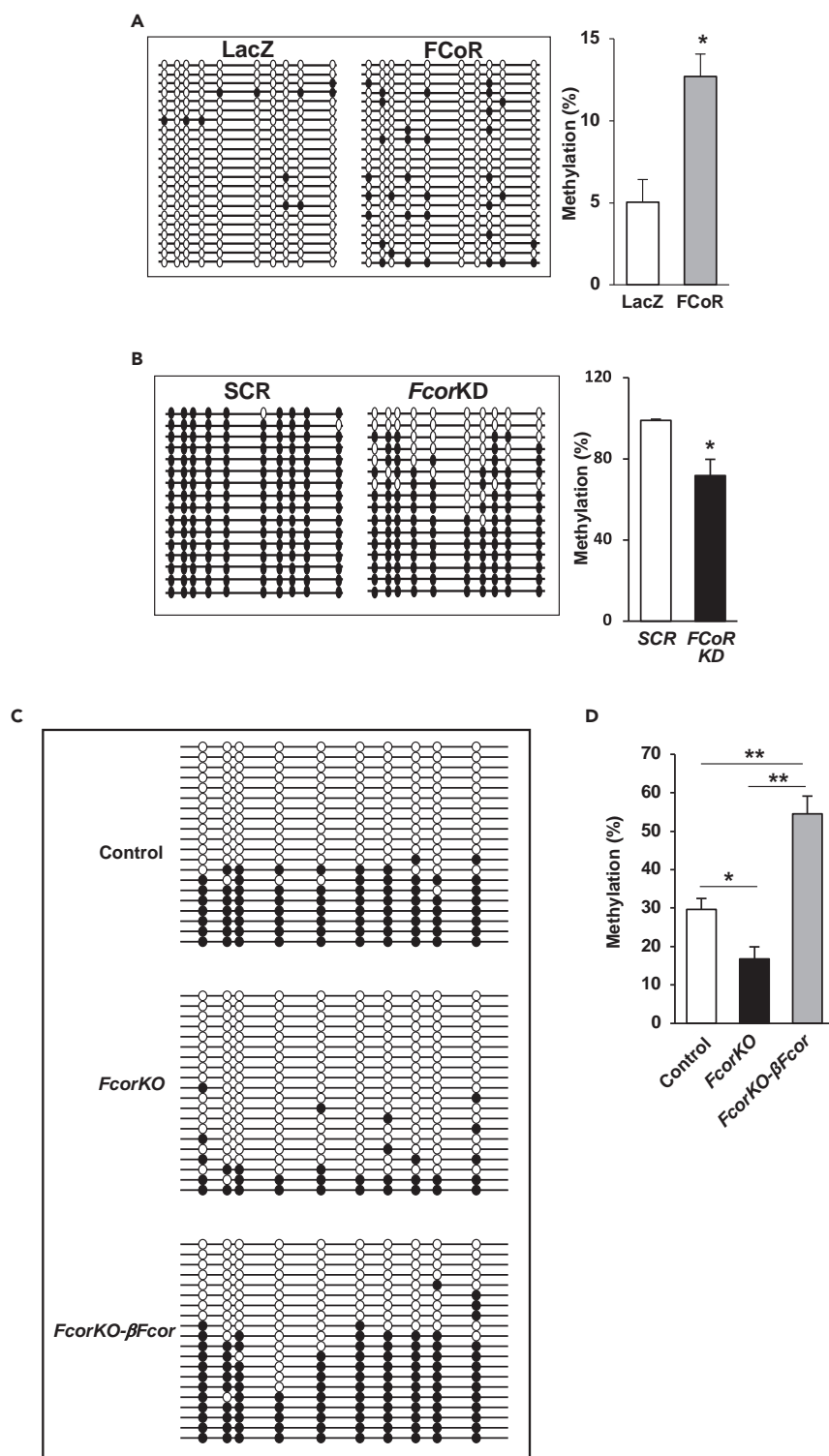
Figure 6. FCoR Regulates DNA Methylation of the *Arx* Promoter

(A) Bisulfite-sequencing analysis of the UR2 region of the *Arx* promoter in αTC1 cells transduced with adenoviruses encoding LacZ (*n* = 45) or FLAG-FCoR (*n* = 50). Quantification of the bisulfite-sequencing data is shown as %DNA methylation.

Figure 6. *Continued*

(B) Bisulfite-sequencing analysis of the UR2 region of the *Arx* promoter in MIN6 cells transduced with adenoviruses encoding shRNA of scramble sequence (SCR) (*n* = 45) or FCoR knockdown sequence (*n* = 50). Quantification of the bisulfite-sequencing data is shown as %DNA methylation. Data represent means ± SEM. *p < 0.05 by one-way ANOVA.

(C and D) Bisulfite-sequencing analysis of the UR2 region of the *Arx* promoter in islets from control (*n* = 12, 263 colonies sequenced), *FcorKO* (*n* = 12, 274 colonies sequenced) and *FcorKO-βFcor* (*n* = 10, 192 colonies sequenced) (C), and quantification of the bisulfite-sequencing data is shown as %DNA methylation (D). Data represent means ± SEM. *p < 0.05 by one-way ANOVA.

These data suggest that FCoR can lead to increased DNA methylation and silent chromatin structure of the UR2 region of *Arx* promoter.

To confirm the effects of FCoR on methylation of the UR2 region of the *Arx* promoter *in vivo*, we performed bisulfite sequencing analysis using islets isolated from control, *FcorKO*, and *FcorKO-βFcor*. Although bisulfite sequencing data using whole islets may be less informative, the size of islets and β-cell mass of *FcorKO* were similar to that of control. Therefore, we thought that whole islets bisulfite sequencing data could indicate endogenous status of DNA methylation of *Arx* promoter in β-cells. Compared with islets from control and *FcorKO-βFcor*, islets from *FcorKO* showed significantly fewer methylated sites (Figures 6C and 6D). Higher DNA methylation in islets isolated from *FcorKO-βFcor* may be the result of excessive expression level of FCoR compared with endogenous FCoR expression level (Figure S2B). These data indicated that FCoR induced methylation of the UR2 region of the *Arx* promoter.

Foxo1 Inhibits Methylation of the *Arx* Promoter

As described above, DNA methylation of *Arx* promoter largely affects *Arx* gene expression level. Therefore, to investigate whether Foxo1 influences DNA methylation of the *Arx* promoter or not, we performed bisulfite sequencing to examine the methylation status of *Arx* promoters from islets isolated from control, *FcorKO*, *DKO*, and *βFoxo1KO*. The results revealed significantly increased methylation of the UR2 region of *Arx* in islets from *βFoxo1KO* compared with control, *FcorKO*, and *DKO*. Methylation of the *Arx* promoter in islets from *DKO* was similar to that of controls and was significantly increased compared with *FcorKO* (Figures 7A and 7B). These data indicated that Foxo1 decreased *Arx* promoter methylation and FCoR inhibits Foxo1-induced *Arx* hypomethylation.

Finally, to examine the molecular mechanism through which Foxo1 decreased methylation of the UR2 region of the *Arx* promoter, we performed a ChIP assay using MIN6 cells transduced with adenoviruses encoding LacZ or HA-ADAFoxo1. Our results showed significantly decreased Dnmt3a binding to the UR2 region in MIN6 cells transduced with adenovirus encoding HA-ADAFoxo1 compared with LacZ (Figure 7C). In contrast, the ChIP assay revealed that FCoR overexpression in αTC1 cells led to increased recruitment of Dnmt3a (but not Dnmt1) to the UR2 region of the *Arx* promoter (Figure 7D). These data indicated that Foxo1 bound to and released Dnmt3a from the UR2 region of the *Arx* promoter and that FCoR increased Dnmt3a recruitment to the UR2 region of the *Arx* promoter, leading to its increased DNA methylation.

DISCUSSION

Our present results confirmed that FCoR plays important roles in the regulation of pancreatic α-cell mass. FCoR expression starts around embryonic day 14.5 in both insulin- and glucagon-positive cells. However, FCoR expression declines in glucagon-positive cells, so that by embryonic day 18.5, it is restricted to insulin-positive cells. This differential pattern promotes increased Arx expression in glucagon-positive cells and decreased Arx expression in insulin-positive cells, resulting in determination of terminally mature endocrine cells.

Of note, FCoR and Foxo1 are expressed in both insulin- and glucagon-positive cells during differentiation. We could not co-stain cells with FCoR and Foxo1 because antibodies for both FCoR and Foxo1 that we used are anti-rabbit antibodies. However, as the developmental phase proceeds, Foxo1 expression becomes restricted in insulin-positive cells, as does FCoR. Interestingly, Foxo1 was strongly co-stained with glucagon-positive cells at embryonic day 15.5, the early phase of endocrine progenitor cells. In contrast, FCoR expression in glucagon-positive cells after embryonic day 14.5 was declined. These data are consistent with the previous report of Foxo1 expression in embryonic glucagon-positive cells (Kitamura et al., 2009) and that Foxo1 may be activated due to loss of FCoR in α-cell-committed cells and facilitate
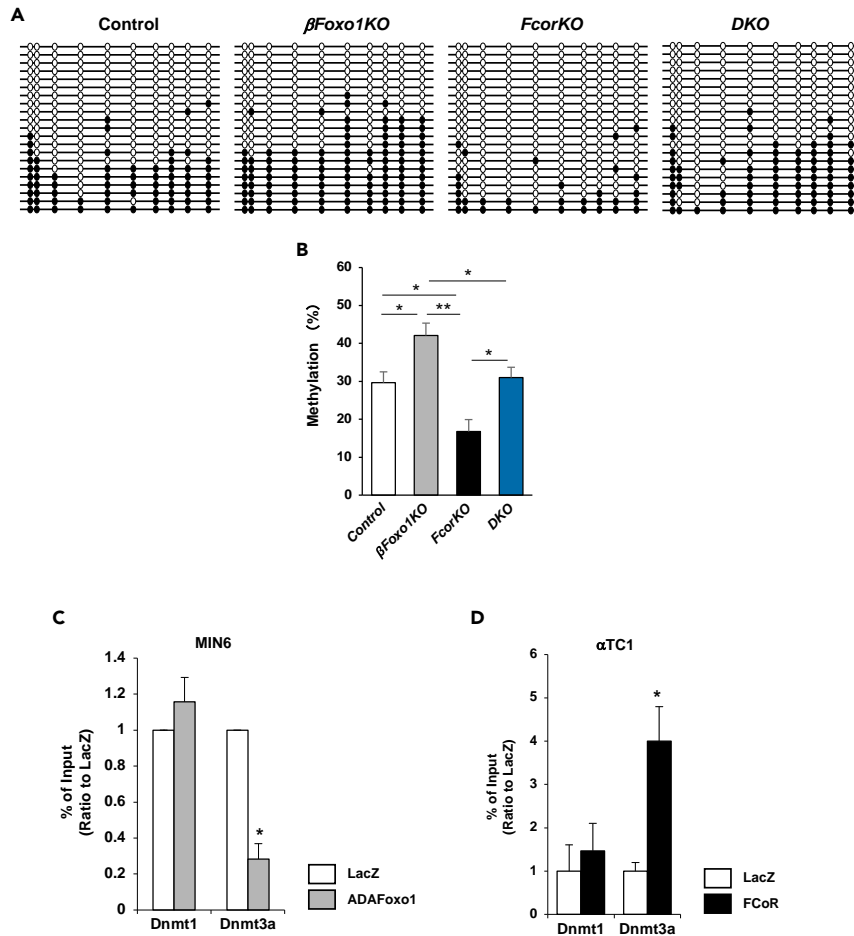
Figure 7. FCoR-Foxo1-regulated Dnmt3a Recruitment to the *Arx* Promoter

(A) Bisulfite-sequencing analysis of the UR2 region of the *Arx* promoter in islets isolated from 20- to 24-week-old control (n = 15, 263 colonies sequenced), *βFoxo1* (n = 10, 157 colonies sequenced), *FcorKO* (n = 15, 274 colonies sequenced), and *DKO* (n = 10, 158 colonies sequenced).

(B) Quantification of the bisulfite-sequencing data is shown as %DNA methylation. Data represent means ± SEM. *p < 0.05 and **p < 0.005 by one-way ANOVA.

(C) ChIP assay of MIN6 cells transduced with adenoviruses encoding LacZ (white bar) or HA-ADA-Foxo1 (gray bar) and harvested at 48 h after transduction. Samples were subjected to immunoprecipitation with anti-DNMT1or anti-DNMT3A, followed by PCR amplification of the UR2 region. Data represent means ± SEM from three independent experiments. *p < 0.05 and **p < 0.005 by one-way ANOVA.

(D) ChIP assay of αTC1 cells transduced with adenoviruses encoding LacZ (white bar) or FLAG-FCoR (black bar) and harvested at 48 h after transduction. Samples were subjected to immunoprecipitation with anti-DNMT1or anti-DNMT3A, followed by PCR amplification of the UR2 region. Data represent means ± SEM from three independent experiments. *p < 0.05 and **p < 0.005 by one-way ANOVA.

α-cell differentiation at early phase of endocrine progenitor cells. FCoR loss results in decreased acetyla-tion and increased activation of Foxo1, namely, increased nuclear Foxo1 because FCoR is a co-repressor and main acetyltransferase for Foxo1 in islets. From the present study, the most important significance of nuclear Foxo1 from *Fcor* loss in pancreatic endocrine cells was the induction of *Arx* expression. Espe-cially, in fetal pancreatic endocrine cells, until embryonic day 14.5, FCoR was expressed in both α- and β-cells. Therefore, FCoR can inactivate Foxo1, and *Arx* expression is suppressed in pancreatic endocrine precursors. However, after embryonic day 14.5, FCoR expression in α-cells gradually declined, leading to Foxo1 activation and *Arx* induction, resulting in fate determination similar to α-cells.

Indeed, loss of *Fcor* causes Foxo1 activation and increased Arx expression in both differentiating pancre-atic α-cells and insulin-positive β-cells, increasing both the α-cell generation and the conversion of β- to

α-cells, ultimately raising the proportion of α-cell mass. However, the architecture of islets from the *FcorKO* genotype is almost normal, indicating the peripheral localization of α-cells. Several cases of β- to α-cell conversion have demonstrated that α-cells are localized in the core of the islets (Lu et al., 2018). Furthermore, the ratio of EGFP-positive cells among glucagon-positive cells was relatively low (2.47%). This low ratio of β-to-α-cell conversion might result from the period of activation of rat insulin promoter in *RIP-Cre* mice. It has been reported that rat insulin promoter was active in terminally differentiated β-cells (Talchai and Accili, 2015). In contrast, *Fcor* deletion is constitutive and occurs before defining a particular cell fate of pancreatic endocrine cells. Therefore, we could detect β-to-α-cell conversion only in adult β-cells. These findings indicate that conversion from β-cells to α-cells in the *FcorKO* genotype might occur in the earlier stages during differentiation of pancreatic endocrine cells and that the architecture of islets therefore should be normal. However, it is also possible that the increase in α-cell mass is due to unrestrained growth of those cells in the earlier stages during differentiation of pancreatic endocrine cells because increased Foxo1 activity due to loss-of-*Fcor* in embryonic α-cells may lead to α-cell hyperplasia (Kitamura et al., 2009), although we could not detect increased proliferation of α-cells in FcorKO at embryonic day 15.5.

The use of *RIP-Cre* to trigger FCoR overexpression specifically in β-cells of *FcorKO* (*FcorKO-βFcor*) normalized the proportion of α-cell mass attributable to the inhibition of *Arx* expression in cells that would otherwise have been converted from β- to α-cells. In contrast, the use of *RIP-Cre* to specifically delete *Foxo1* in terminally differentiated β-cells does not alter the proportion of α-cells (Talchai and Accili, 2015) because decreased *Arx* expression due to loss-of-*Foxo1* from terminally differentiated β-cells does not influence the β-cell fate. On the other hand, in *αFcor*, FCoR overexpression in glucagon-positive cells significantly decreased the α-cell mass compared with controls. This effect may become manifest just before the establishment of differentiated pancreatic endocrine cells, because endogenous glucagon-positive cells are reportedly detectable at embryonic day 9.5, before detection of the first insulin-positive cells at embryonic day 10.5–11 (Herrera et al., 2002). These findings suggest that FCoR overexpression using *Glucagon-Cre* leads to a decrease in the α-cell lineage itself and thus to a significantly decreased α-cell mass compared with controls. Of interest, *DKO* mice exhibited significantly greater α-cell mass compared with controls, although *Arx* expression level was normalized. Because *FcorKO* represents null knockout mice, in these animals, deletion of *Fcor* has occurred not only in the β-cell lineage but also in the α-cell lineage, resulting in increased α-cell lineage during fetal development of pancreatic endocrine cells. Therefore, even if deletion of *Foxo1* specifically in *Fcor*-deleted β-cells prevents β-to-α-cell conversion, it does not affect α-cell lineage increases. These data indicate that FCoR regulates *Arx* expression through Foxo1. However, we cannot exclude the possibility that other factors mediate the function of FCoR in islets. Further investigation should be needed.

During the development of pancreatic endocrine cells, next to Ngn3 induction, a complex network of transcription factors, including Arx and Pax4, differentially promotes the specific endocrine fates. These two transcription factors, Arx and Pax4, have mutually antagonistic effects. The amount of *Pax4* expression is up-regulated in *Arx* mutant mice, whereas the *Arx* expression is increased in *Pax4*-deficient pancreas (Collombat et al., 2003). This is consistent with the present study. *Pax4* expression in *FcorKO* islets was significantly decreased compared with control islets. Furthermore, overexpression of FCoR in αTC1 cells significantly increased *Pax4* expression but decreased *Arx* expression. In contrast, knockdown of *Fcor* in MIN6 cells significantly increased *Arx* expression but decreased *Pax4* expression. However, interestingly, *FcorKO* islets exhibit significantly increased expression of mature β-cell markers, including *Pdx1*, *Mafa*, *Neurod*, and *Ucn3*, even if *Pax4* expression is decreased. These findings in *FcorKO* islets are not consistent with decreased *Mafa* expression in *Fcor*-knockdowned-MIN6 cells. We speculate that decreased *Mafa* expression in *Fcor*-knockdowned-MIN6 cells is an acute effect of *Fcor* knockdown but that *Fcor* deletion in *FcorKO* is constitutive and has chronic effects on gene expression in islets, leading to compensatory induction of mature β-cell markers. Indeed, *Mafa* expression is regulated by several transcription factors, including *Foxa2*, *Nkx2.2*, and *Pdx1*, and glucose levels (Vanderford, 2011). Therefore, chronic effects resulting from *Fcor* deletion may affect expression levels of mature β-cell markers because null *FcorKO* exhibits glucose intolerance due to insulin resistance in adipose tissues (Nakae et al., 2012). Furthermore, these findings might indicate that the effect on glucose-stimulated insulin secretion in *FcorKO* may come from an α-cell-centric phenotype and these changes in β-cell-maturity-markers may be compensatory, resulting in the generation of dysfunctional α-cells, or the generation of dysfunctional β-cells, leading to decreased

insulin secretion. Indeed, bihormonal or immature cells were increased significantly in islets of *FcorKO* compared with control. However, further investigation is needed to elucidate the precise molecular mechanism by which loss-of-*Fcor* induces the generation of dysfunctional β-cells. Furthermore, as already reported, activation of Foxo1 in pancreatic β-cells leads to protection of β-cells against oxidative stress through formation of a complex with the promyelocytic leukemia protein Pml and Sirt1 to activate expression of *Mafa* and *Neurod* (Kitamura et al., 2005) (Kobayashi et al., 2012). This finding is consistent with our present data, which indicate increased expression levels of *Mafa* and *Neurod* in islets isolated from *FcorKO*.

The molecular mechanism by which DNA methylation regulates *Arx* expression has been reported. In one proposed model, a repressor complex that includes Nkx2.2, Grg3, and Dnmt3a preferentially recruits HDAC1 to the *Arx* promoter to silence *Arx* expression specifically in the pancreatic β-cells, preventing β-to-α-cell conversion (Dhawan et al., 2011; Papizan et al., 2011). Of interest, the FRE in the *Arx* promoter is close to the consensus Nkx2.2-binding site (Figure S8A). The binding of Foxo1 to the FRE may dissociate the repressor complex from the *Arx* promoter, leading to *Arx* promoter hypomethylation and induction of *Arx* expression. In contrast, inhibition of Foxo1 by FCoR may make the repressor complex assemble on the *Arx* promoter, leading to hypermethylation as shown in the present study. Furthermore, our present findings confirmed that the binding of Foxo1 to the *Arx* promoter led to Dnmt3a dissociation from the *Arx* promoter. However, we performed bisulfite sequencing analysis using whole islets from each genotype. Therefore, these data may be affected by differences in the α-/β-cell ratios. But, because β-cell mass of each genotype is similar and the absolute value of α-cell mass is relatively low, the differences of α-/ β-cell ratios may slightly affect the results of bisulfite sequencing data.

In the present study, the findings of significantly decreased acetylation of transduced Foxo1 in *FcorKO* islets are notable. Deacetylated Foxo1 can be imported to the nucleus, where it can bind to the FREs of its target genes, and should be active transcriptionally (Matsuzaki et al., 2005) (Qiang et al., 2010). The main acetyltransferases of Foxo1 are reported to be CBP, p300, and PCAF (Brunet et al., 2004) (Motta et al., 2004) (Yoshimochi et al., 2010). However, little is known about the regulation of Foxo1 acetylation in islets, although the mechanism by which Foxo1 in islets is deacetylated is well described (Kitamura et al., 2005). The present data indicate that FCoR is one of the regulators of Foxo1 acetylation in islets and works upstream of Foxo1.

In conclusion, here we provide evidence that the FCoR-Foxo1 axis is an important determinant in regulating the identities of pancreatic α-cell. Elucidating the molecular mechanisms underlying the regulation of α- and β-cell masses will be an important step toward developing strategies to cure diabetes. Our present findings indicate that FCoR offers a promising target molecule for the development of therapies for type 2 diabetes.

Limitations of the Study
In the present study, we demonstrated that FCoR increased DNA methylation of *Arx* promoter using the whole islets. However, to clarify DNA methylation of *Arx* promoter in β-cells, we should perform bisulfite sequencing analysis using the sorted β-cells. Furthermore, ChIP analysis of Dnmt3a should be performed using isolated islets. These experiments will reveal the conversion of β- to α-cells more precisely.

METHODS
All methods can be found in the accompanying Transparent Methods supplemental file.

SUPPLEMENTAL INFORMATION
Supplemental Information can be found online at https://doi.org/10.1016/j.isci.2019.100798.

ACKNOWLEDGMENTS

AUTHOR CONTRIBUTIONS

DECLARATION OF INTERESTS

REFERENCES

Accili, D., and Arden, K.C. (2004). FoxOs at the crossroads of cellular metabolism, differentiation, and transformation. Cell 117, 421–426.

Banks, A.S., Kim-Muller, J.Y., Mastracci, T.L., Kofler, N.M., Qiang, L., Haeusler, R.A., Jurczak, M.J., Laznik, D., Heinrich, G., Samuel, V.T., et al. (2011). Dissociation of the glucose and lipid regulatory functions of FoxO1 by targeted knockin of acetylation-defective alleles in mice. Cell Metab. 14, 587–597.

Berger, S.L. (2007). The complex language of chromatin regulation during transcription. Nature 447, 407–412.

Bouchi, R., Foo, K.S., Hua, H., Tsuchiya, K., Ohmura, Y., Sandoval, P.R., Ratner, L.E., Egli, D., Leibel, R.L., and Accili, D. (2014). FOXO1 inhibition yields functional insulin-producing cells in human gut organoid cultures. Nat. Commun. 5, 4242.

Brunet, A., Sweeney, L.B., Sturgill, J.F., Chua, K.F., Greer, P.L., Lin, Y., Tran, H., Ross, S.E., Mostoslavsky, R., Cohen, H.Y., et al. (2004). Stress-dependent regulation of FOXO transcription factors by the SIRT1 deacetylase. Science 303, 2011–2015.

Collombat, P., Hecksher-Sorensen, J., Broccoli, V., Krull, J., Ponte, I., Mundiger, T., Smith, J., Gruss, P., Serup, P., and Mansouri, A. (2005). The simultaneous loss of Arx and Pax4 genes promotes a somatostatin-producing cell fate specification at the expense of the alpha- and beta-cell lineages in the mouse endocrine pancreas. Development 132, 2969–2980.

Collombat, P., Hecksher-Sorensen, J., Serup, P., and Mansouri, A. (2006). Specifying pancreatic endocrine cell fates. Mech. Dev. 123, 501–512.

Collombat, P., Mansouri, A., Hecksher-Sorensen, J., Serup, P., Krull, J., Gradwohl, G., and Gruss, P. (2003). Opposing actions of Arx and Pax4 in endocrine pancreas development. Genes Dev. 17, 2591–2603.

Collombat, P., Xu, X., Ravassard, P., Sosa-Pineda, B., Dussaud, S., Billestrup, N., Madsen, O.D., Serup, P., Heimberg, H., and Mansouri, A. (2009). The ectopic expression of Pax4 in the mouse pancreas converts progenitor cells into alpha and subsequently beta cells. Cell 138, 449–462.

Courtney, M., Gjernes, E., Druelle, N., Ravaud, C., Vieira, A., Ben-Othman, N., Pfeifer, A., Avolio, F., Leuckx, G., Lacas-Gervais, S., et al. (2013). The inactivation of Arx in pancreatic alpha-cells triggers their neogenesis and conversion into functional beta-like cells. PLoS Genet. 9, e1003934.

Dhawan, S., Georgia, S., Tschen, S.I., Fan, G., and Bhushan, A. (2011). Pancreatic beta cell identity is maintained by DNA methylation-mediated repression of Arx. Dev. Cell 20, 419–429.

Dor, Y., and Glaser, B. (2013). Beta-cell dedifferentiation and type 2 diabetes. N. Engl. J. Med. 368, 572–573.

Dunning, B.E., and Gerich, J.E. (2007). The role of alpha-cell dysregulation in fasting and postprandial hyperglycemia in type 2 diabetes and therapeutic implications. Endocr. Rev. 28, 253–283.

Frescas, D., Valenti, L., and Accili, D. (2005). Nuclear trapping of the forkhead transcription factor FoxO1 via Sirt-dependent deacetylation promotes expression of glucogenetic genes. J. Biol. Chem. 280, 20589–20595.

Gao, T., McKenna, B., Li, C., Reichert, M., Nguyen, J., Singh, T., Yang, C., Pannikar, A., Doliba, N., Zhang, T., et al. (2014). Pdx1 maintains beta cell identity and function by repressing an alpha cell program. Cell Metab. 19, 259–271.

Habener, J.F., Kemp, D.M., and Thomas, M.K. (2005). Minireview: transcriptional regulation in pancreatic development. Endocrinology 146, 1025–1034.

Herrera, P.L., Nepote, V., and Delacour, A. (2002). Pancreatic cell lineage analyses in mice. Endocrine 19, 267–278.

Kitamura, T., Kitamura, Y.I., Kobayashi, M., Kikuchi, O., Sasaki, T., Depinho, R.A., and Accili, D. (2009). Regulation of pancreatic juxtaductal endocrine cell formation by FoxO1. Mol. Cell. Biol. 29, 4417–4430.

Kitamura, Y.I., Kitamura, T., Kruse, J.P., Raum, J.C., Stein, R., Gu, W., and Accili, D. (2005). FoxO1 protects against pancreatic beta cell failure through NeuroD and MafA induction. Cell Metab. 2, 153–163.

Kobayashi, M., Kikuchi, O., Sasaki, T., Kim, H.J., Yokota-Hashimoto, H., Lee, Y.S., Amano, K., Kitazumi, T., Susanti, V.Y., Kitamura, Y.I., et al. (2012). FoxO1 as a double-edged sword in the pancreas: analysis of pancreas- and beta-cell-specific FoxO1 knockout mice. Am. J. Physiol. Endocrinol. Metab. 302, E603–E613.

Kouzarides, T. (2007). Chromatin modifications and their function. Cell 128, 693–705.

Lu, T.T., Heyne, S., Dror, E., Casas, E., Leonhardt, L., Boenke, T., Yang, C.H., Sagar, L., Arrigoni, L., Dalgaard, K., et al. (2018). The Polycomb-dependent epigenome controls beta cell dysfunction, dedifferentiation, and diabetes. Cell Metab. 27, 1294–1308.e7.

Martin, C., and Zhang, Y. (2007). Mechanisms of epigenetic inheritance. Curr. Opin. Cell Biol. 19, 266–272.

Matsuzaki, H., Daitoku, H., Hatta, M., Aoyama, H., Yoshimochi, K., and Fukamizu, A. (2005). Acetylation of Foxo1 alters its DNA-binding ability and sensitivity to phosphorylation. Proc. Natl. Acad. Sci. U S A 102, 11278–11283.

Menge, B.A., Gruber, L., Jorgensen, S.M., Deacon, C.F., Schmidt, W.E., Veldhuis, J.D., Holst, J.J., and Meier, J.J. (2011). Loss of inverse relationship between pulsatile insulin and

glucagon secretion in patients with type 2 diabetes. Diabetes 60, 2160–2168.

Mihaylova, M.M., Vasquez, D.S., Ravnskjaer, K., Denechaud, P.D., Yu, R.T., Alvarez, J.G., Downes, M., Evans, R.M., Montminy, M., and Shaw, R.J. (2011). Class IIa histone deacetylases are hormone-activated regulators of FOXO and mammalian glucose homeostasis. Cell 145, 607–621.

Motta, M.C., Divecha, N., Lemieux, M., Kamel, C., Chen, D., Gu, W., Bultsma, Y., McBurney, M., and Guarente, L. (2004). Mammalian SIRT1 represses forkhead transcription factors. Cell 116, 551–563.

Nakae, J., Cao, Y., Daitoku, H., Fukamizu, A., Ogawa, W., Yano, Y., and Hayashi, Y. (2006). The LXXLL motif of murine forkhead transcription factor FoxO1 mediates Sirt1-dependent transcriptional activity. J. Clin. Invest. 116, 2473–2483.

Nakae, J., Cao, Y., Hakuno, F., Takemori, H., Kawano, Y., Sekioka, R., Abe, T., Kiyonari, H., Tanaka, T., Sakai, J., et al. (2012). Novel repressor regulates insulin sensitivity through interaction with Foxo1. EMBO J. 31, 2275–2295.

Nakae, J., Kitamura, T., Silver, D.L., and Accili, D. (2001). The forkhead transcription factor Foxo1 (Fkhr) confers insulin sensitivity onto glucose-6-phosphatase expression. J. Clin. Invest. 108, 1359–1367.

Papizan, J.B., Singer, R.A., Tschen, S.I., Dhawan, S., Friel, J.M., Hipkens, S.B., Magnuson, M.A., Bhushan, A., and Sussel, L. (2011). Nkx2.2 repressor complex regulates islet beta-cell specification and prevents beta-to-alpha-cell reprogramming. Genes Dev. 25, 2291–2305.

Puri, S., and Hebrok, M. (2010). Cellular plasticity within the pancreas–lessons learned from development. Dev. Cell 18, 342–356.

Qiang, L., Banks, A.S., and Accili, D. (2010). Uncoupling of acetylation from phosphorylation regulates FoxO1 function independent of its subcellular localization. J. Biol. Chem. 285, 27396–27401.

Rukstalis, J.M., and Habener, J.F. (2009). Neurogenin3: a master regulator of pancreatic islet differentiation and regeneration. Islets 1, 177–184.

Talchai, C., Xuan, S., Kitamura, T., DePinho, R.A., and Accili, D. (2012a). Generation of functional insulin-producing cells in the gut by Foxo1 ablation. Nat. Genet. 44, 406–412, S1.

Talchai, C., Xuan, S., Lin, H.V., Sussel, L., and Accili, D. (2012b). Pancreatic beta cell dedifferentiation as a mechanism of diabetic beta cell failure. Cell 150, 1223–1234.

Talchai, S.C., and Accili, D. (2015). Legacy effect of Foxo1 in pancreatic endocrine progenitors on adult beta-cell mass and function. Diabetes 64, 2868–2879.

Thorel, F., Nepote, V., Avril, I., Kohno, K., Desgraz, R., Chera, S., and Herrera, P.L. (2010). Conversion of adult pancreatic alpha-cells to beta-cells after extreme beta-cell loss. Nature 464, 1149–1154.

Vanderford, N.L. (2011). Regulation of beta-cell-specific and glucose-dependent MafA expression. Islets 3, 35–37.

Wang, B., Moya, N., Niessen, S., Hoover, H., Mihaylova, M.M., Shaw, R.J., Yates, J.R., 3rd, Fischer, W.H., Thomas, J.B., and Montminy, M. (2011). A hormone-dependent module regulating energy balance. Cell 145, 596–606.

Yoshimochi, K., Daitoku, H., and Fukamizu, A. (2010). PCAF represses transactivation function of FOXO1 in an acetyltransferase-independent manner. J. Recept. Signal Transduct. Res. 30, 43–49.

Ziv, O., Glaser, B., and Dor, Y. (2013). The plastic pancreas. Dev. Cell 26, 3–7.

Supplemental Information

FCoR-Foxo1 Axis Regulates α-Cell

Mass through Repression of *Arx* Expression

Noriko Kodani, Jun Nakae, Masaki Kobayashi, Osamu Kikuchi, Tadahiro Kitamura, and Hiroshi Itoh

Transparent Methods

Antibodies and Cell Cultures

Anti-FCoR antiserum has been described previously (Nakae et al., 2012). We purchased anti-FLAG (M2) and anti-tubulin from Sigma; anti-cMyc (9E10) from Santa Cruz Biotechnology, Inc; anti-FOXO1 (L27) and anti-acetylated lysine polyclonal antibodies from Cell Signaling Technology; anti-insulin from Dako; and anti-glucagon (ab92517) from Abcam. Anti-Arx antibody was a gift from Dr. Ken-ichirou Morohashi and Dr. Kanako Miyabayashi (Kyushu University, Fukuoka, Japan) (Kitamura et al., 2002) (Miyabayashi et al., 2013), and anti-EGFP was a gift from Dr. Naoki Mochizuki (National Cerebral and Cardiovascular Center, Osaka, Japan). Anti-DNMT1 (60B1220.1) was purchased from Novus Biological; anti-DNMT3A (ab13888) from Abcam; anti-Sirt1 (07-131) from Merck Millipore; anti-HA (12CA5) from Santa Cruz Biotechnology, Inc.; anti-MeCP2 (#3456) from Cell Signaling; anti-Histone H3 (tri methyl K4) (ab213224) from Abcam; anti-Histone H3 (tri methyl K9) (ab176916) from Abcam; and anti-Ki67 (RM-9106-S1) from Thermo Fisher Scientific. HEK293, αTC1, and MIN6 cells were cultured as described previously (Nakae et al., 1999) (Efrat et al., 1988) (Ishihara et al., 1993).

Available Mice

RIP-Cre(Herrera, 2000), Glucagon-Cre (Herrera, 2000), FcorKO (Nakae et al., 2012), Foxo1$^{flox/flox}$ (Paik et al., 2007), and CAG-CAT-EGFP (Kawamoto et al., 2000) mice have been previously described elsewhere. Foxo1$^{flox/flox}$ mice were obtained from Dr. Ronald DePinho, University of Texas M.D. Anderson Cancer Center, courtesy of Dr. Domenico Accili, Columbia University.

Animal Studies, Analytical Procedures, and Intraperitoneal Glucose and Insulin Tolerance Tests

For the following experiments, we used only male mice, which are more susceptible to insulin resistance and diabetes. All experimental protocols using mice were approved by the animal ethics committee of the Keio University School of Medicine. Animals were fed a standard chow diet and water ad libitum, and were housed in sterile cages in a barrier animal facility with a 12-h light/12-h dark cycle. Wild-type littermates were used as controls. At weaning (4 weeks of age), the mice were started on a high-fat diet (HFD). We continued to provide the same diet, and blood glucose and insulin level measurements and glucose and insulin tolerance tests were performed as described previously (Nakae et al., 2008). All assays were performed in duplicate, and each value represents the mean of two independent determinations.

Generation of Tissue-specific FCoR Transgenic Mice

We ligated a BspE1-BamHI-BglII adaptor (5'-CCGGAGGATCCA-3') with pAcGFP1-C1 (Clontech) treated with BspE1 and BglII. We amplified a BglII- and EcoRI-treated PCR fragment using 5'-GGGGAGATCTATGGACTACAAAGACGATGAC-3' and 5'-GGGGGAATTCCTAGCACATGCCTTTAGTCCC-3', with pFLAG-CMV2-FCoR (Nakae et al., 2012) as a template, and ligated this fragment with BglII- and EcoRI-treated pAcGFP1-C1 (pAcGFP1-C1-FLAG-FCoR). Next, EcoRI- and SmaI-treated β-globin pA of the pBS II SK(+)-CAG-CAT-EGFP vector (Kawamoto et al., 2000) was ligated with EcoRI- and SmaI-treated pAcGFP1-C1-FLAG-FCoR (pAcGFP1-C1-FLAG-FCoR- β-globin pA). Finally, the BamHI-treated pAcGFP1-C1-FLAG-FCoR- β-globin pA fragment was ligated with the BamHI-treated pBS II SK(+)-CAG-CAT-EGFP vector. The transgene was excised using SalI and SacI, gel-purified, and injected into fertilized eggs from BDF1 x C57BL/6 mice. The resulting embryos were implanted into CD-1 foster mothers, and the offspring were screened for transgene transmission by PCR. Ten independent transgenic lines were obtained, among which seven founders transmitted the transgene through the germ line. To obtain F1 mice, we crossed each founder with C57BL/6 mice. We then crossed the F1 mice with Albumin-Cre transgenic mice (Okamoto et al., 2007). We sacrificed one mouse from each line in which the transgene was transmitted, and examined the transgene expression in the liver. We ultimately obtained two independent *Fcor* transgenic lines. The primers used for genotyping were: 5'- ATG GAC TAC AAA GAC GAT GAC –3' and 5'-CTGCACCGGTCTCATCCTTTC-3'.

RNA Isolation and Real-time PCR

We isolated total RNA from tissues and cells using the SV Total RNA Isolation System (Promega) following the manufacturer's protocol. Real-time PCR was performed as previously described(Nakae et al., 2008). The primers used in this study are described in Supplementary Table 1.

Insulin and Glucagon Secretion Studies

Pancreatic islets were isolated by collagenase digestion. The isolated pancreatic islets were preincubated for 15 min in KREBS buffer (119 mM NaCl; 2.5mM $CaCl_2$; 1.19mM KH_2PO_4; 1.19mM $MgSO_4$; 10mM HEPES, pH 7.4; and 2% bovine serum albumin) with 2.8 mM glucose, and then stimulated for 1 h with glucose or L-arginine at the indicated concentration. We measured the insulin and glucagon released in the incubation buffer using the rat insulin radioimmunoassay kit (RI-13K, Millipore) and glucagon

radioimmunoassay kit (GL-32K, Millipore), respectively. The amounts of insulin secretion were normalized according to the cellular DNA content. For measurement of islet insulin content, islets were solubilized in acid-ethanol solution (74% ethanol, 1.4% HCl) overnight at 4°C before insulin measurement. The amounts of insulin content were normalized according to the numbers of islets.

Bisulfite Sequencing Analysis

Bisulfite conversion of DNA isolated from αTC1 or MIN6 cells, or from isolated male mice pancreatic islets, was subjected to bisulfite conversion using the EZ DNA Methylation™ Kit (Zymo Research). Bisulfite-treated DNA samples were used for PCR using Arx UR2 primers(Dhawan et al., 2011). PCR products were gel purified using the QIAquick® Gel Extraction Kit (QUIAGEN). Purified products were cloned using the Mighty TA-cloning Kit (Takara), and sequenced using the BigDye® Terminator v3.1 Cycle Sequencing Kit (Thermo Fisher) with the M13 Primer RV (CAGGAAACAGCTATGAC).

Chromatin Immunoprecipitation (ChIP) Assay

αTC1 or MIN6 cells were seeded onto 10 cm-culture dishes and transduced with adenovirus encoding constitutively nuclear HA-tagged ADA-Foxo1. At 36-48 h after transduction, the cells were fixed with 1% formaldehyde at 37°C for 1 h. The DNA solution for ChIP PCR was prepared according to the protocol for the Chip Assay Kit (Upstate). Immunoprecipitation was performed using anti-HA (12CA5; Santa Cruz Biotechnology, Inc.), anti-MeCP2 (#3456; Cell Signaling), anti-Histone H3 (tri methyl K4) (ab213224, Abcam), anti-Histone H3 (tri methyl K9) (ab176916, Abcam), anti-DNMT1 (60B1220.1, Novus Biological), anti-DNMT3A (ab13888, Abcam), or an equal amount of normal mouse IgG (Santa Cruz Biotechnology, Inc). Samples were subjected to PCR amplification of the UR2 region of the *Arx* promoter(Dhawan et al., 2011).

Construction of Arx Promoter-directed Luciferase Reporter Vectors

From mouse genomic DNA, we PCR amplified several DNA fragments containing the mouse *Arx* promoter using the following primers: forward primers, *1813Ccr2* 5'-GGGGAGATCTTCCACCATTTGAGGGTACGGAAAAC-3' and *1432Ccr2* 5'-GGGGAGATCTAGAGAGGAAAACCTGGCGTGGATT-3' (underlining indicates the BglII recognition site); reverse primer, 5'- GGGGAAGCTT GGCTGGTGCTTTTTCCTTGGGCTC -3' (underlining indicates the HindIII recognition site). Their nucleotide sequences were verified by DNA sequencing. Then the *Arx* promoter fragments were treated with BglII- and HindIII-treated luciferase reporter pGL3-

Basic vector (Promega, Madison, WI).

Site-directed Mutagenesis

To alter the consensus Foxo1 response element (FRE) in the *Arx* promoter of the PGL3-Basic vectors, we performed site-directed mutagenesis using the QuickChange II site-directed mutagenesis kit (Stratagene, La Jolla, CA). The Mutant 1 vector was constructed using the following primers: 5'-ATCCAAGAGTTATGCAGA**TG**GGGA**TGGCTGGGGGGGAAAAATC-3' and 5'-GATTTTTCCCCCCAGCCA**TCCC**C**A**TCTGCATAACTCTTGGAT-3' (mutant bases are indicated by bold font and underlining). The Mutant 2 vector was constructed using the following two primers: 5'-ATCCAAGAGTTATGCAGA**GGGGGA**TGGCTGGGGGGGAAAAATC-3' and 5'-GATTTTTCCCCCCAGCCA**TCCC**C**C**TCTGCATAACTCTTGGAT-3' (mutant bases are indicated by bold font and underlining). The Mutant 3 vector was constructed using the following two primers: 5'-ATCCAAGAGTTATGCAGA**GGGGGG**TGGCTGGGGGGGAAAAATC-3' and 5'-GATTTTTCCCCCCAGCCA**CCCC**C**C**TCTGCATAACTCTTGGAT-3' (mutant bases are indicated by bold font and underlining). Mutated nucleotides were confirmed by DNA sequencing.

Luciferase Assay

For the mouse *Arx* promoter luciferase assay, MIN6 cells were plated onto 12-well culture dishes. Cells were grown to 70%-80% confluence, and transfections were performed using 1.5μg of pGL3/Basic-*Arx* reporter vector, and/or 0.6μg of pFLAG-CMV-2 empty vector or constitutively nuclear FLAG-CMV-2-CNFoxo1 expression vectors(Nakae et al., 2006). The synthetic renilla luciferase reporter vector (phRL-SV40; Promega) (10ng) was used as an internal control of transfection efficiency. After transfection, cells were cultured in DMEM containing 15% foetal calf serum and 0.0005% β-mercaptoethanol. Following a 36-h incubation, the cells were harvested for the luciferase assay.

Electrophoretic Mobility Shift Assay (EMSA)

From HEK293T cells transfected with PCMV5/cMyc-WTFoxo1, we isolated nuclear extracts using the NE-PER extraction reagents (Pierce). The DNA probe was a 31-bp DNA fragment covering the consensus FRE (-1565/-1535 nt) of the mouse *Arx* promoter: (5'-AGAGTTATGCAGA<u>TGTTTA</u>TGGCTGGGGGGA-3'). The mutant probe contained five bases substitutions within the consensus FRE (underlined letters): 5'-

AGAGTTATGCAGA<u>GGGGGG</u>TGGCTGGGGGGA -3'. The oligonucleotides were labelled with ^{32}P-ATP using the MEGALABEL[TM] DNA 5'-End Labeling Kit (Takara Bio, Inc., Shiga, Japan). EMSA was performed as previously described(Nakae et al., 2003). For the super shift assay, we incubated anti-cMyc or normal mouse IgG with nuclear extracts at 4°C for 20 min, added labeled probes, and performed another 20-min incubation at room temperature. Competitor wild-type and mutant probes were incubated in the reaction mixture for 20 min prior to the addition of the radiolabelled probe.

Construction of Adenoviral Vectors and Adenoviral Transduction
Previous reports describe the adenoviral vectors encoding cMyc-FCoR (Nakae et al., 2012) or HA-ADA-Foxo1 (Nakae et al., 2001), and the adenovirus vectors for FCoR knockdown(Nakae et al., 2012). To construct an adenoviral vector encoding FCoR, we amplified the FLAG-FCoR cDNA fragment using the pFLAG-CMV2-FCoR expression vector (Nakae et al., 2012) as a template and the following primers: 5' - GG GCTAGC (NheI) ATGGACTACAAAGACGATGACGAC-3' (sense) and 5'-GG GCTAGC (NheI) CTAGCACATGCCTTTAGTCCC-3' (antisense). After treatment with NheI, the PCR fragment was subcloned into a NheI-treated pShuttle2 vector (Clontech). Following sequencing of the vectors to confirm that they had the intended sequences, and confirming protein expression in HEK293 by transient transfection, a fragment treated with I-CeuI- and PI-SceI was subcloned into Adeno-X viral DNA (pAdeno-X-FLAG-FCoR) (Clontech). The adenovirus vector was generated by transfecting HEK293 cells with the pAdeno-X-FLAG-FCoR plasmid. αTC1 or MIN6 cells were grown to 70%-80% confluence, and then transduced every day with adenovirus preparations encoding cMyc-FCoR, FLAG-FCoR, or FCoR-shRNA at different MOI for 7-8 h and removed from the culture dish. The cells were harvested after 48 h.

Western Blotting
We homogenized tissues and lysed cells in buffer containing 50mM Tris HCl (pH 8.0), 250mM NaCl, 1% NP40, 0.5% deoxycholate, 0.1% SDS, and protease inhibitors (Roche Diagnostics). The lysis solution was centrifuged to remove insoluble material, and the proteins in 30 μg of lysate were separated using 8% or 14 % SDS-PAGE. Western blotting was performed using the indicated antibodies. Immunoprecipitation was performed as previously described (Cao et al., 2006).

Immunohistochemistry, Immunofluorescence and Histological Analysis
For histological analysis, dissected pancreases were fixed in 10 % paraformaldehyde

and embedded in paraffin blocks. Tissues were cut in 5µm section by a microtome and used for immunohistochemical staining. 4 pancreatic sections from 3-7 mice from each genotype were sampled 150-200 µm apart. For α- and β-cell, each section was covered systematically by accumulating images from non-overlapping fields with fluorescence microscope (BZ-9000, KEYENCE) using a 10 x objective for whole pancreas sections. All morphometric analyses were performed using ImageJ software. Briefly, individual channels were converted to 8 bits grayscale and measurement scale was converted from pixels to microns. An identical threshold was applied to all images from the same channel to exclude background signals and further converted to binary format before automated analysis of weight. Sections in the lineage tracing study were imaged on Olympus Fluoview V3000 confocal microscope or KEYENCE BZ-X800 fluorescent microscope at 400X. Z-stack images were taken using KEYENCE BZ-X800 and was transformed into 3D images.

Statistical Analysis

We calculated descriptive statistics using one-way ANOVA with the Fisher's test. All data are expressed as mean $\pm$ standard error. Significance was set at $p < 0.05$.

SUPPLEMENTAL REFERENCES

Cao, Y., Kamioka, Y., Yokoi, N., Kobayashi, T., Hino, O., Onodera, M., Mochizuki, N., and Nakae, J. (2006). Interaction of FoxO1 and TSC2 induces insulin resistance through activation of the mammalian target of rapamycin/p70 S6K pathway. J Biol Chem *281*, 40242-40251.

Dhawan, S., Georgia, S., Tschen, S.I., Fan, G., and Bhushan, A. (2011). Pancreatic beta cell identity is maintained by DNA methylation-mediated repression of Arx. Dev Cell *20*, 419-429.

Efrat, S., Linde, S., Kofod, H., Spector, D., Delannoy, M., Grant, S., Hanahan, D., and Baekkeskov, S. (1988). Beta-cell lines derived from transgenic mice expressing a hybrid insulin gene-oncogene. Proc Natl Acad Sci U S A *85*, 9037-9041.

Herrera, P.L. (2000). Adult insulin- and glucagon-producing cells differentiate from two independent cell lineages. Development *127*, 2317-2322.

Ishihara, H., Asano, T., Tsukuda, K., Katagiri, H., Inukai, K., Anai, M., Kikuchi, M., Yazaki, Y., Miyazaki, J.I., and Oka, Y. (1993). Pancreatic beta cell line MIN6 exhibits characteristics of glucose metabolism and glucose-stimulated insulin secretion similar to those of normal islets. Diabetologia *36*, 1139-1145.

Kawamoto, S., Niwa, H., Tashiro, F., Sano, S., Kondoh, G., Takeda, J., Tabayashi, K.,

and Miyazaki, J. (2000). A novel reporter mouse strain that expresses enhanced green fluorescent protein upon Cre-mediated recombination. FEBS Lett *470*, 263-268.

Kitamura, K., Yanazawa, M., Sugiyama, N., Miura, H., Iizuka-Kogo, A., Kusaka, M., Omichi, K., Suzuki, R., Kato-Fukui, Y., Kamiirisa, K., et al. (2002). Mutation of ARX causes abnormal development of forebrain and testes in mice and X-linked lissencephaly with abnormal genitalia in humans. Nat Genet *32*, 359-369.

Miyabayashi, K., Katoh-Fukui, Y., Ogawa, H., Baba, T., Shima, Y., Sugiyama, N., Kitamura, K., and Morohashi, K. (2013). Aristaless related homeobox gene, Arx, is implicated in mouse fetal Leydig cell differentiation possibly through expressing in the progenitor cells. PLoS One *8*, e68050.

Nakae, J., Cao, Y., Daitoku, H., Fukamizu, A., Ogawa, W., Yano, Y., and Hayashi, Y. (2006). The LXXLL motif of murine forkhead transcription factor FoxO1 mediates Sirt1-dependent transcriptional activity. J Clin Invest *116*, 2473-2483.

Nakae, J., Cao, Y., Hakuno, F., Takemori, H., Kawano, Y., Sekioka, R., Abe, T., Kiyonari, H., Tanaka, T., Sakai, J., et al. (2012). Novel repressor regulates insulin sensitivity through interaction with Foxo1. EMBO J *31*, 2275-2295.

Nakae, J., Cao, Y., Oki, M., Orba, Y., Sawa, H., Kiyonari, H., Iskandar, K., Suga, K., Lombes, M., and Hayashi, Y. (2008). Forkhead transcription factor FoxO1 in adipose tissue regulates energy storage and expenditure. Diabetes *57*, 563-576.

Nakae, J., Kitamura, T., Kitamura, Y., Biggs, W.H., 3rd, Arden, K.C., and Accili, D. (2003). The forkhead transcription factor Foxo1 regulates adipocyte differentiation. Dev Cell *4*, 119-129.

Nakae, J., Kitamura, T., Silver, D.L., and Accili, D. (2001). The forkhead transcription factor Foxo1 (Fkhr) confers insulin sensitivity onto glucose-6-phosphatase expression. J Clin Invest *108*, 1359-1367.

Nakae, J., Park, B.C., and Accili, D. (1999). Insulin stimulates phosphorylation of the forkhead transcription factor FKHR on serine 253 through a Wortmannin-sensitive pathway. J Biol Chem *274*, 15982-15985.

Okamoto, Y., Ogawa, W., Nishizawa, A., Inoue, H., Teshigawara, K., Kinoshita, S., Matsuki, Y., Watanabe, E., Hiramatsu, R., Sakaue, H., et al. (2007). Restoration of glucokinase expression in the liver normalizes postprandial glucose disposal in mice with hepatic deficiency of PDK1. Diabetes *56*, 1000-1009.

Paik, J.H., Kollipara, R., Chu, G., Ji, H., Xiao, Y., Ding, Z., Miao, L., Tothova, Z., Horner, J.W., Carrasco, D.R., et al. (2007). FoxOs Are Lineage-Restricted Redundant Tumor Suppressors and Regulate Endothelial Cell Homeostasis. Cell *128*, 309-323.
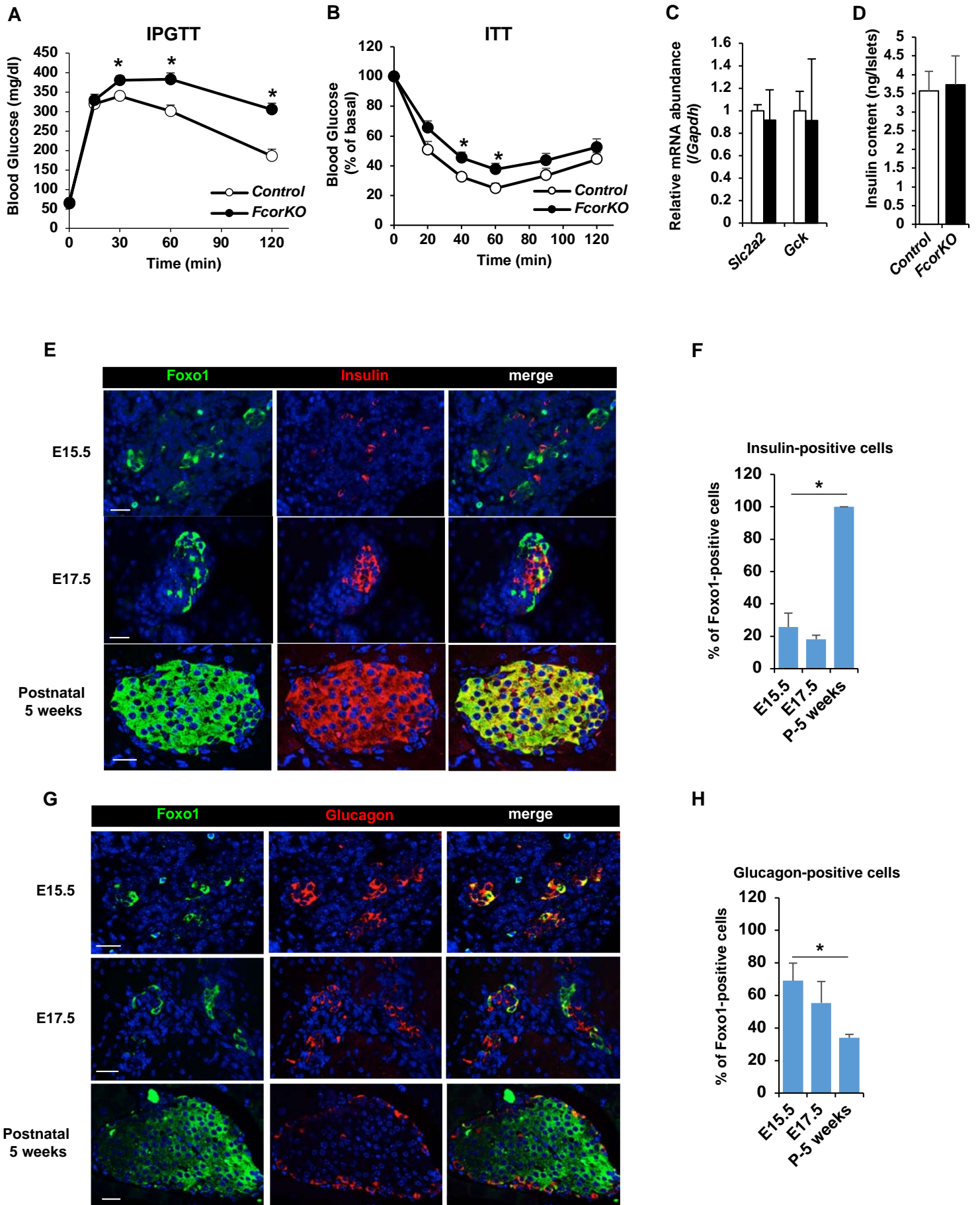
Figure S1

Figure S1. Related to Figure 1. Glucose Metabolism and Foxo1 Expression in Fetal Pancreas.
(A) Intraperitoneal glucose tolerance test (IPGTT) of control (n=11) and *FcorKO* (n=12) at the age
of 20 weeks. Data are means $\pm$ SEM. *$P < 0.05$ by two-way ANOVA with Fisher's test.
(B) Insulin tolerance test (ITT) of control (n=11) and *FcorKO* (n=14) at the age of 20 weeks.
Data are represented as % of basal glucose level and means $\pm$ SEM. *$P < 0.05$ by two-way ANOVA
with Fisher's test.
(C) Expression levels of Glut 2 (*Slc2a2*) and Glucokinase (*Gck*) in islets isolated from control
(white bar) (n=4) and *FcorKO* (black bar) (n=4) at the age of 20-24 weeks.
Data represent means $\pm$ SEM.
(D) Insulin content of islets isolated from control (n=4) and *FcorKO* (n=4) at the age of 20-24 weeks.
Data are represented as insulin content (ng) per islet and means $\pm$ SEM.
(E)(F) Representative images of pancreatic islets for Foxo1 and insulin from embryos (n=3) at
embryonic days 15.5 (E15.5), 17.5 (E17.5), and postnatal week 5 (E) and the percentages of
Foxo1-positive cells among insulin-positive cells (F). Data represent means $\pm$ SEM.
* $P <0.05$ by one-way ANOVA. Scale bar, 20 μm.
(G)(H) Representative images of pancreatic islets for Foxo1 and glucagon from embryos (n=3)
at embryonic days 15.5 (E15.5), 17.5 (E17.5), and postnatal week 5 (G) and the percentages of
Foxo1-positive cells among glucagon-positive cells (H). Data represent means $\pm$ SEM.
* $P <0.05$ by one-way ANOVA. Scale bar, 20 μm.

A

β-cell targeting

βFcor

RIP → Cre

CAG → CAT → FLAG-Fcor — β-globin pA

B

	1	2	3
FCoR			
FLAG			
Tubulin			

1: control
2: *βFcor*
3: *αFcor*

C

| Control | *βFcor* |
| FLAG Glucagon DAPI | |

D

Fcor+/-

CAG → CAT → FLAG-Fcor — β-globin pA

✕

Fcor+/-

RIP → Cre

↓

FcorKO

FcorKO-βFcor

RIP → Cre

CAG → CAT → FLAG-Fcor — β-globin pA
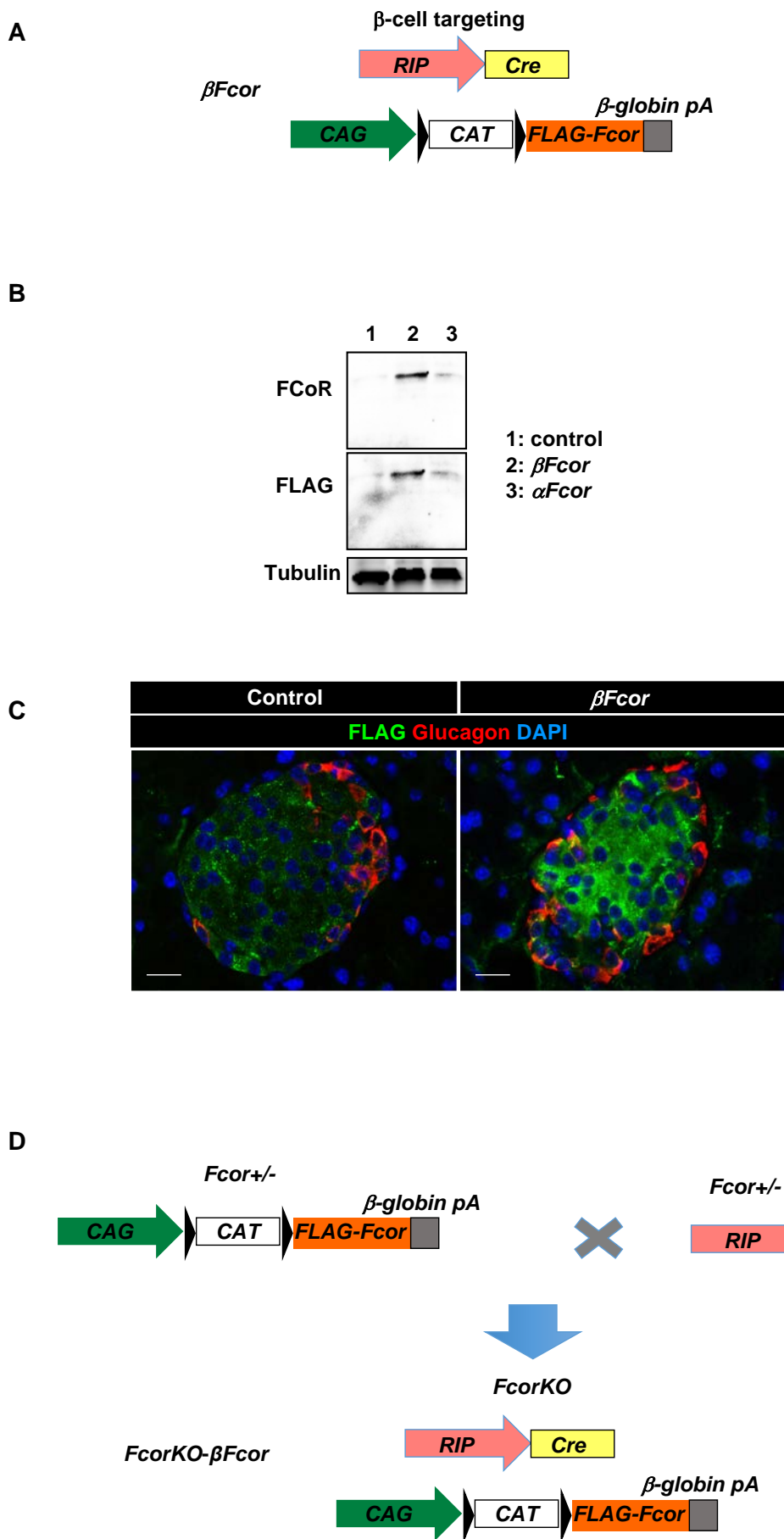
Figure S2

Figure S2. Related to Figure 2. Generation of β-Cell-Specific *Fcor* Transgenic Mice
(A) Construction of β-cell-specific *Fcor* transgenic mice (*βFcor*).
(B) Western blotting of islets isolated from control, *βFcor,* and *αFcor* with anti-FCoR, anti-FLAG, and anti-tubulin antibodies.
(C) Representative images of immunofluorescence of islets from control and *βFcor* using anti-FLAG and anti-glucagon antibodies. Scale bar, 20μm.
(D) Generation of *FcorKO-βFcor*.

A

α-cell targeting

αFcor

Glucagon *Cre*

β-globin pA

CAG *CAT* *FLAG-Fcor*

B

| Control | *αFcor* |

FLAG Glucagon DAPI

C

α-cell mass

β-cell mass

D
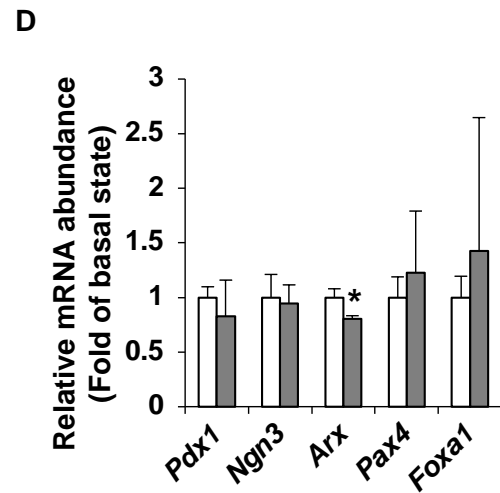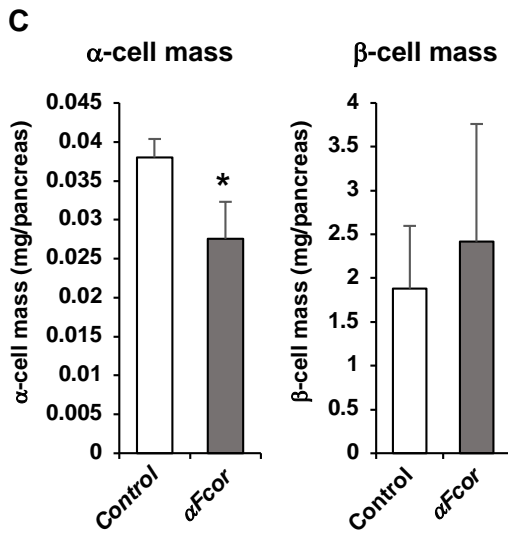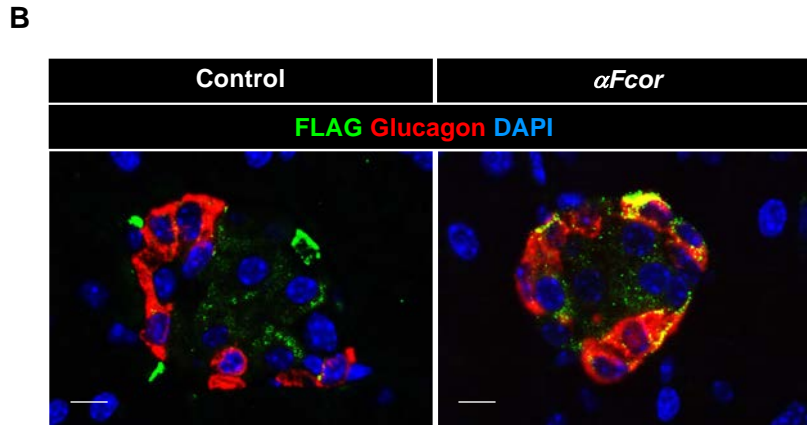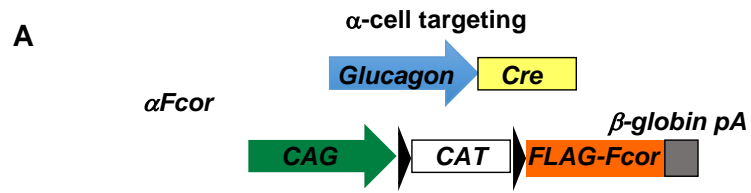
Figure S3

Figure S3. Related to Figure 2. Generation of α-Cell-Specific *Fcor* Transgenic Mice
(A) Construction of α-cell-specific *Fcor* transgenic mice (*αFcor*).
(B) Representative images of immunofluorescence of islets from control and *αFcor* using anti-FLAG and anti-glucagon antibodies. Scale bar, 10μm.
(C) Quantification of α-cell and β-cell mass in control (n=7 mice; 174 islets measured) and *αFcor* (n=5 mice; 166 islets measured).
(D) Gene expression in islets isolated from control (white bar) and *αFcor* (gray bar).
Data represent means ± SEM from three independent experiments. *P<0.05 by one-way ANOVA.
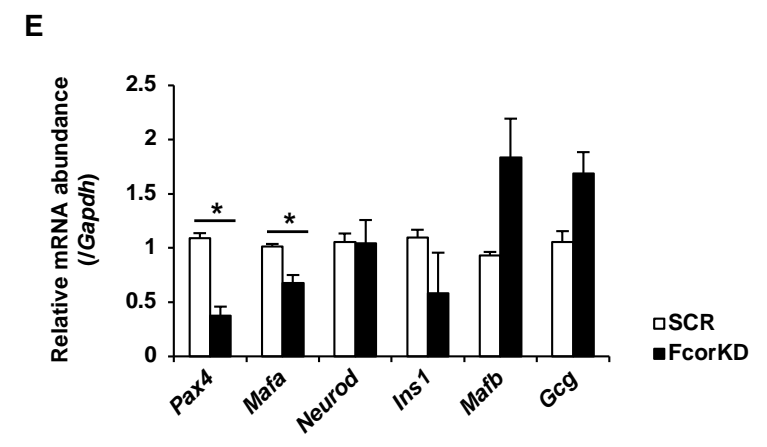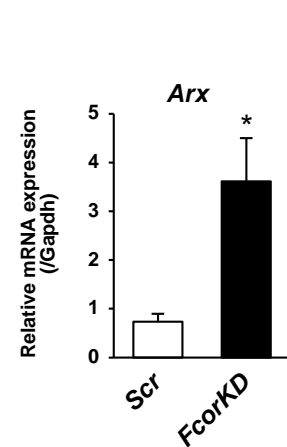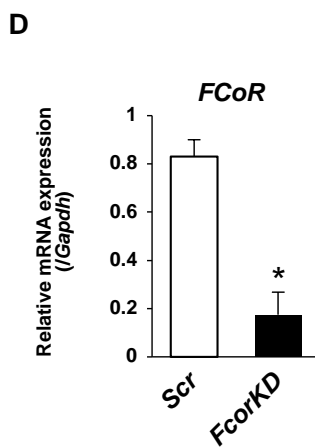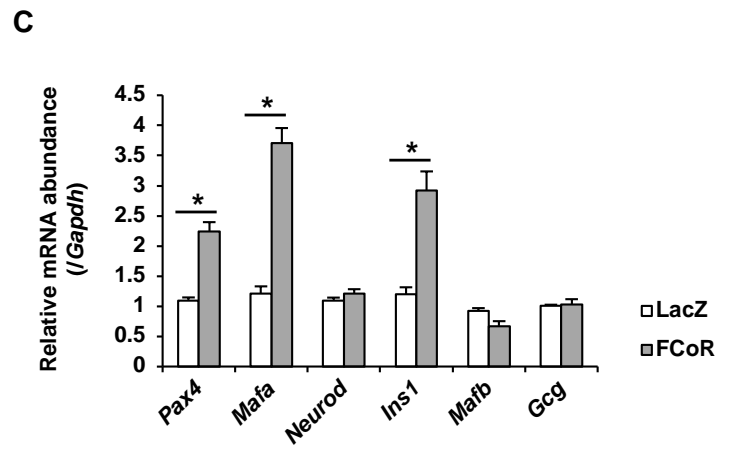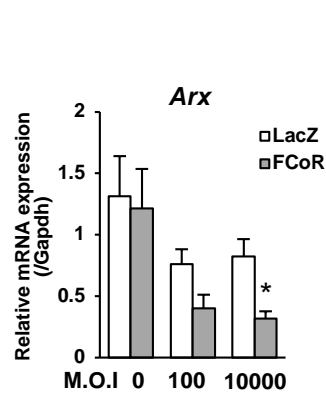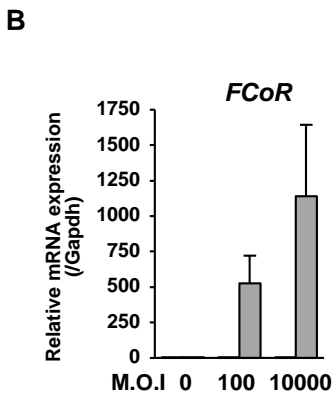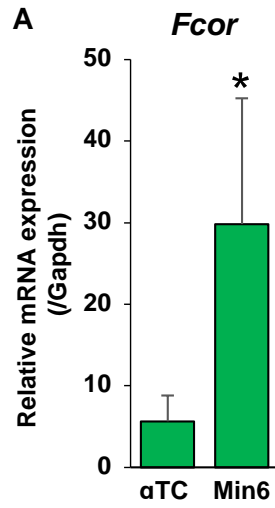
Figure S4

Figure S4. Related to Figure 2. Endogenous Expression Levels of Islet-specific Genes in Cell Lines.

(A) *Fcor* Expression in αTC1 and MIN6 Cells. *Fcor* expression in αTC1 and MIN6 cells. Data represent means $\pm$ SEM from three independent experiments. *P<0.05 by one-way ANOVA.

(B) *Fcor* and *Arx* expression in αTC1 cells transduced with adenoviruses encoding LacZ (white bar) and FLAG-FCoR (gray bar). Data represent means $\pm$ SEM from three independent experiments. *P<0.05 by one-way ANOVA.

(C) Expression levels of islet-specific genes in αTC1 cells transduced with adenoviruses encoding LacZ (white bar) and FLAG-FCoR (grey bar). Data represent means $\pm$ SEM from three independent experiments. *P<0.05 by one-way ANOVA.

(D) The effect of FCoR knockdown on *Arx* expression in MIN6 cells. *Fcor* and *Arx* expression in MIN6 cells transduced with adenoviruses encoding scramble-shRNA (*Scr*) (white bar) and *Fcor* knockdown-shRNA (*FcorKD*) (black bar). Data represent means $\pm$ SEM from three independent experiments. *P<0.05 by one-way ANOVA.
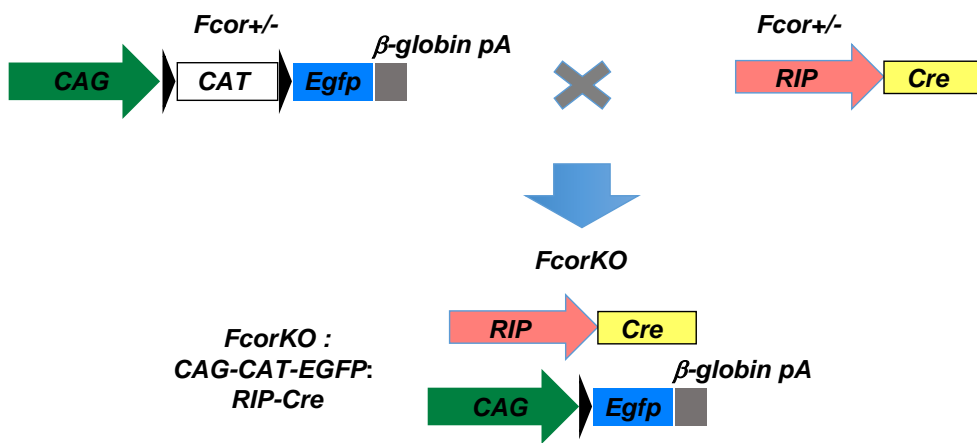
(E) Expression levels of islet-specific genes in MIN6 cells transduced with adenoviruses encoding scramble-shRNA (*Scr*) (white bar) and *Fcor* knockdown-shRNA (*FcorKD*) (black bar). Data represent means $\pm$ SEM from three independent experiments. *P<0.05 by one-way ANOVA.

Fcor+/-

CAG | CAT | Egfp | *β-globin pA*

✕

Fcor+/-

RIP | Cre

↓

FcorKO

FcorKO :
CAG-CAT-EGFP:
RIP-Cre

RIP | Cre

CAG | Egfp | *β-globin pA*

Figure S5. Related to Figure 3. β-Cell Tracing Analysis of *FcorKO*
Construction of β-cell tracing mice.
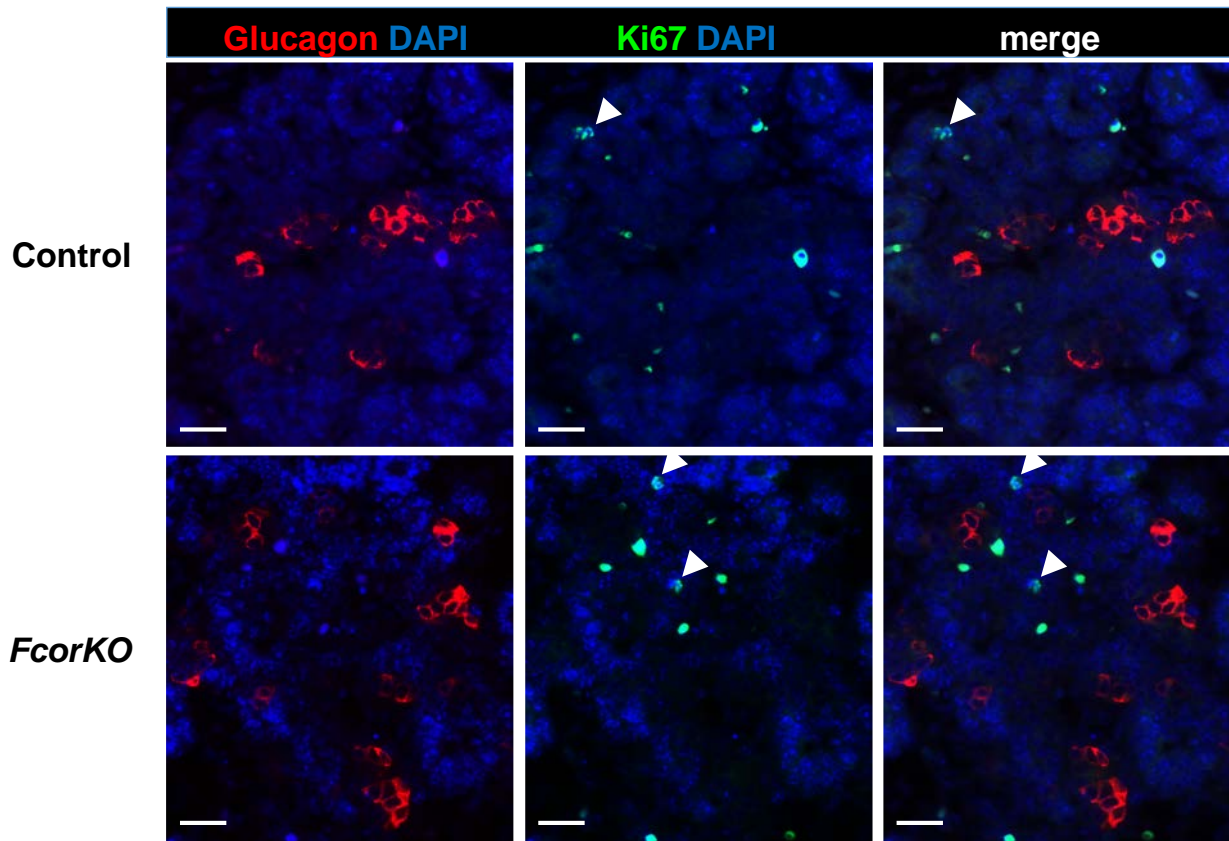
| Glucagon DAPI | Ki67 DAPI | merge |

Control

FcorKO

Figure S6. Related to Figure 3. Glucagon and Ki67 staining of fetal pancreas from control and *FcorKO*.

Representative images of fetal pancreas for glucagon and Ki67 from control and *FcorKO* at embryonic day 15.5. Scale bar, 20µm.
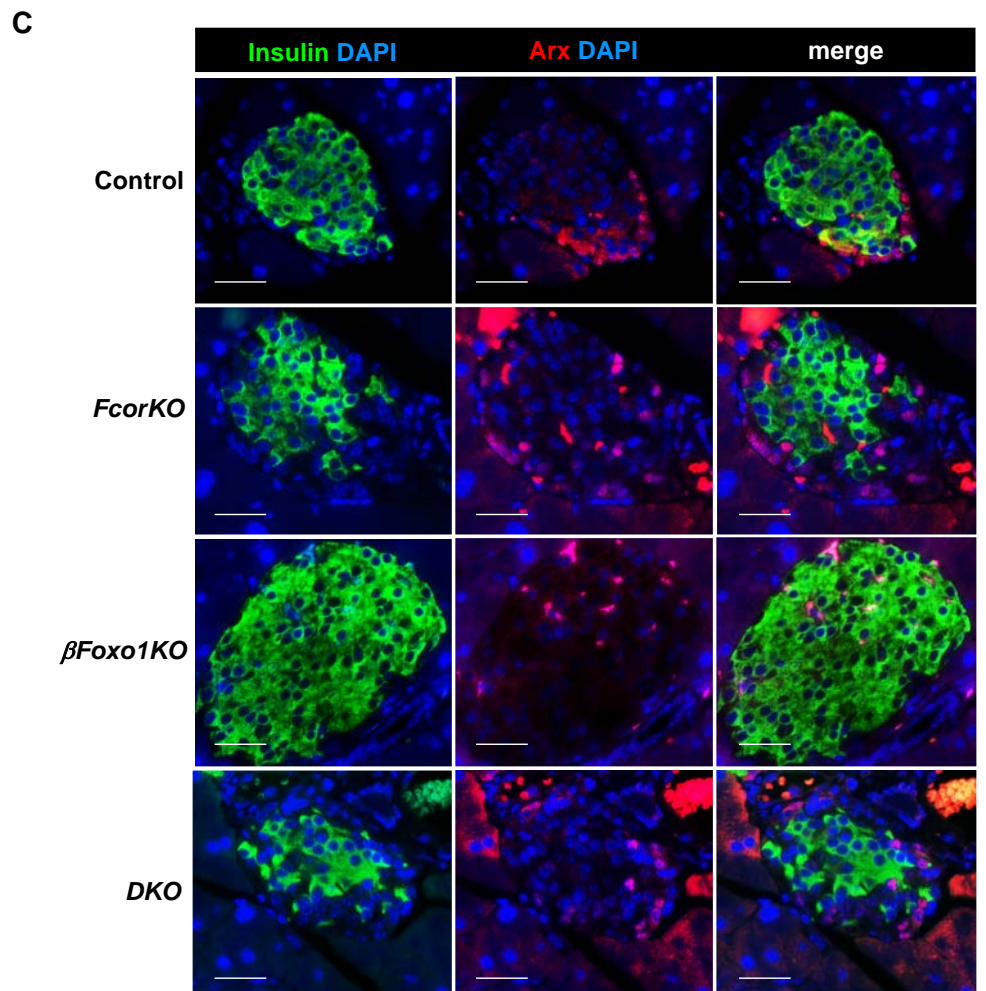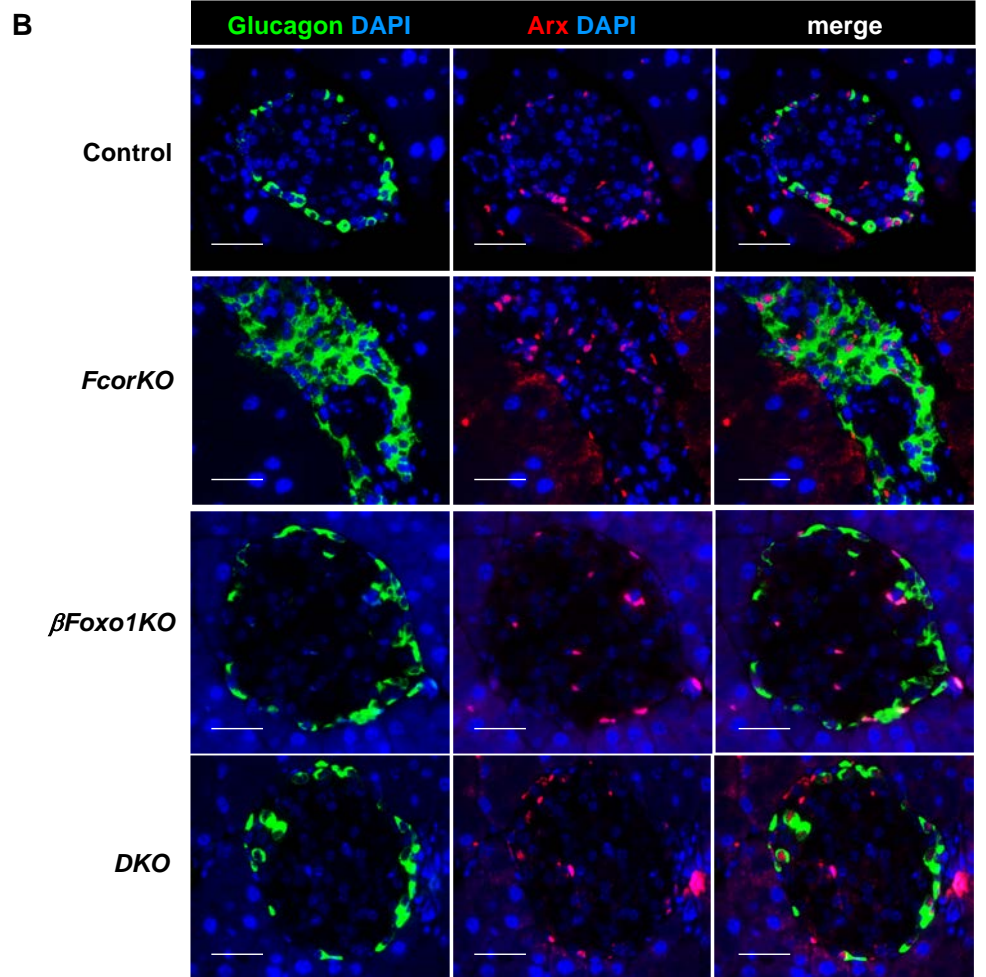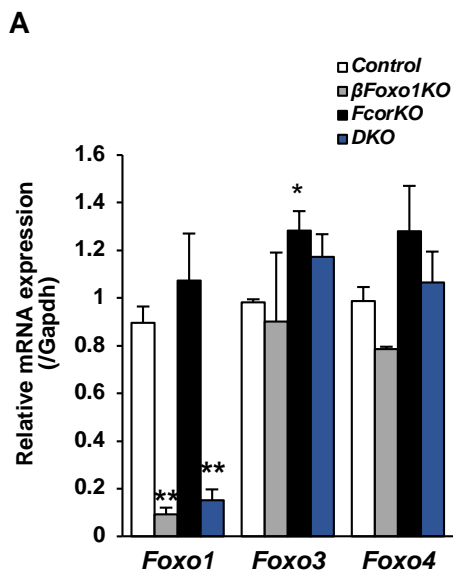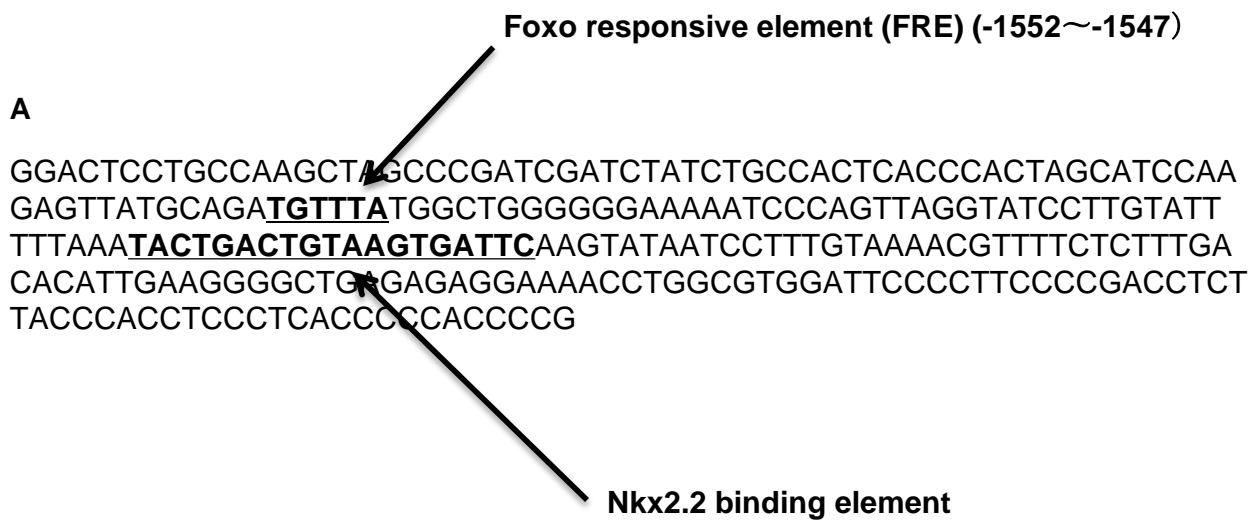
Figure S7

Figure S7. Related to Figure 5. Expression of *Foxo* Family Genes and Arx in Islets.
(A) Gene Expression Levels of *Foxo* Family Members in Islets. Gene expression levels of *Foxo* family members in islets isolated from 16-week-old controls (n=4), *FcorKO* (n=4), *DKO* (n=4), and *βFoxo1KO* (n=4). Data represent means ± SEM from three independent experiments. *P<0.05, and **P<0.005 by one-way ANOVA.
(B, C) Arx expression in islets from control, *FcorKO*, *βFoxo1KO*, *DKO*.
Representative images of pancreatic islets for Arx and glucagon (B), or Arx and insulin (C) from control, *FcorKO*, *βFoxo1KO*, *DKO* at the age of 24 weeks. Scale bar, 50 μm.

Foxo responsive element (FRE) (-1552～-1547）

A

GGACTCCTGCCAAGCTAGCCCGATCGATCTATCTGCCACTCACCCACTAGCATCCAA
GAGTTATGCAGA**TGTTTA**TGGCTGGGGGGAAAAATCCCAGTTAGGTATCCTTGTATT
TTTAAA**TACTGACTGTAAGTGATTC**AAGTATAATCCTTTGTAAAACGTTTTCTCTTTGA
CACATTGAAGGGGCTGAGAGAGGAAAACCTGGCGTGGATTCCCCTTCCCCGACCTCT
TACCCACCTCCCTCACCCCCACCCCG

Nkx2.2 binding element

B

FRE(-1576～-1571）

Human *ARX* GAGTTATGCAGATGTTTATGGCTGAAAAAAAAAAATCCCAGTTATGCATCCTTGTAT

Mouse *Arx* GAGTTATGCAGATGTTTATGGCTGGGGGGGAAAAATCCCAGTTAGGTATCCTTGTATT

FRE(-1552～-1547）

Figure S8

Figure S8. Related to Figure 6. Analysis of Mouse *Arx* Promoter Region
(A) Sequencing data of the *Arx* promoter region around the Foxo responsive element
and NKX2.2 binding element.
(B) Conservation between human and mouse sequences of the *Arx* promoter region near the Foxo
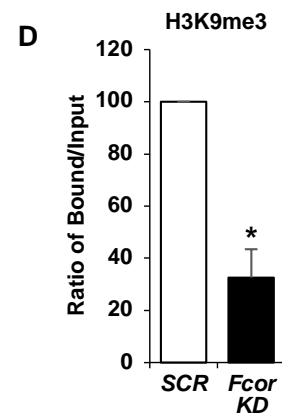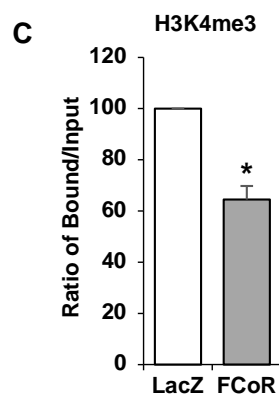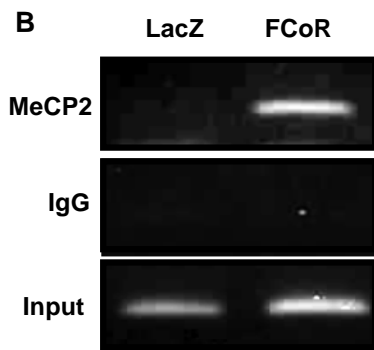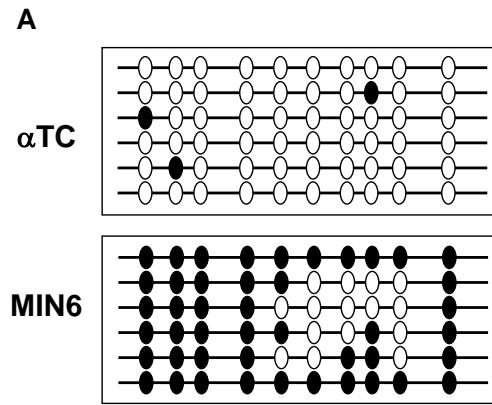responsive element (FRE).

A

αTC

MIN6

B

	LacZ	FCoR
MeCP2		
IgG		
Input		

C

H3K4me3

Ratio of Bound/Input

120
100
80
60
40
20
0

LacZ   FCoR

*

D

H3K9me3

Ratio of Bound/Input

120
100
80
60
40
20
0

SCR   Fcor
KD

*

Figure S9

Figure S9. Related to Figure 4. DNA Methylation and Histone Modification of *Arx* Promoter Region.

(A) Methylation Status of the UR2 Region of the *Arx* Promoter in αTC1 and MIN6 Cells. Bisulfite sequencing analysis of the UR2 region of *Arx* promoter in αTC1 and MIN6 cells.

(B) ChIP assay showing the binding of MeCP2 to the UR2 region of *Arx* promoter in αTC1 cells transduced with adenoviruses encoding LacZ or FLAG-FCoR, and harvested 48 h after transduction.

(C)(D) ChIP assay comparing the levels of H3K4 trimethylation (H3K4me3) (C) and H3K9 trimethylation (H3K9me3) (D) at the UR2 region of the Arx promoter in αTC1 cells transduced with adenoviruses encoding LacZ or FCoR (C), and in MIN6 cells transduced with adenoviruses encoding scramble shRNA (SCR) or *Fcor*-knockdown shRNA (*Fcor KD*) (D).

Data represent means ± SEM from three independent experiments. *P<0.05 by one-way ANOVA.

Table S1. Related to Figure 2. Primers used for real-time PCR

Gene symbol	Sense	Antisense
Arx	GGCCGGAGTGCAAGAGTAAAT	TCGATGCAGTAGGAGGAGAGC
Pax4	AGGGGGACTCTTTGTGAATGG	ACCTGTGCGGTAGTAGCGT
Pdx1	TTCCCGAATGGAACCGAGC	GCGTGAGCTTTGGTGGATT
Slc2a2	TCAGAAGACAAGATCACCGGA	TCAGAAGACAAGATCACCGGA
Mafa	AGGAGGAGGTCATCCGACTG	CTTCTCGCTCTCCAGAATGTG
Neurod	ATGACCAAATCATACAGCGAGAG	TCTGCCTCGTGTTCCTCGT
Ucn3	AAGCCTCTCCCACAAGTTCTA	GAGGTGCGTTTGGTTGTCATC
Ins1	CACTTCCTACCCCTGCTGG	ACCACAAAGATGCTGTTTGACA
Ins2	GCTTCTTCTACACACCCATGTC	AGCACTGATCTACAATGCCAC
Neurog3	AGTGCTCAGTTCCAATTCCAC	CGGCTTCTTCGCTTTTTGCTG
Gcg	GATCATTCCCAGCTTCCCAG	CTGGTAAAGGTCCCTTCAGC
Irx1	CTGGGCTACCCGCAATACC	ATACATGCCTAGCACCGAGGT
Irx2	CCAAGCCCGTAACCTCCTC	GTCCGACGTGGCTATCTCG
Mafb	TTCGACCTTCTCAAGTTCGACG	GAGATGGGTCTTCGGTTCAGT
Foxa1	ATGAGAGCAACGACTGGAACA	TCATGGAGTTCATAGAGCCCA
Fcor	AATGCTTAGGAGGCCCTTCCA	CGGTGCAGTTCCCAGCCCTAC
Dnmt1	AAGAATGGTGTTGTCTACCGAC	CATCCAGGTTGCTCCCCTTG
Dnmt3a	GAGGGAACTGAGACCCCAC	CTGGAAGGTGAGTCTTGGCA
Tet1	ACACAGTGGTGCTAATGCAG	AGCATGAACGGGAGAATCGG
Tet2	AGAGAAGACAATCGAGAAGTCGG	CCTTCCGTACTCCCAAACTCAT
Foxo1	GTCCTGGGCCAAAATGTAATG	AGCCTGACACCCAGCTGTGTG
Foxo3a	CAAACGGCTCACTTTGTCCC	GGTTGATGATCCACCAAGAGCT
Foxo4	TGACACTCGCCCAGATCTACG	AGGACAGGTTGTGACGGATGG
Gapdh	CATCTTGGGCTACACTGAGGA	TGGAGGCCATGTAGGCCATGA